Chapter 3: JOINT PERFORMANCE TEST SETUPS AND EVALUATION PROCEDURES

3.1 Introduction

A joint performance component has not yet been incorporated in any of the currently available whitetopping design procedures. Probably, the complexity involved in its characterization is the reason for being neglected. Most of the research studies (Colley & Humphrey, 1967; Nowlen, 1968; Bruinsma, et al., 1995 Raja & Snyder, 1995 and Jensen & Hansen, 2001 and Brink, et al., 2004) that characterized the joint performance in conventional concrete pavements were carried out by casting large size slabs. Joint performance characterization with large size slabs is expensive and generally cost-prohibitive, when evaluating the joint performance with respect to a large number of variables. Therefore, development of a simple, economic and accurate joint performance test procedure is a dire necessity. The present study developed a small-scale joint performance test. As mentioned in Chapter 1, this procedure is referred as the 'beam accelerated load testing' (B_{ALT}) procedure.

The procedures for estimating the joint performance characterizing parameters such as LTE and DER are also established in this study. The results obtained from the B_{ALT} procedure is then compared and correlated with the results from a large-scale joint performance test. The large-scale procedure is referred as to the 'slab accelerated load testing' (S_{ALT}). Although the joint performance testing with a large size slab is not new, the setup used to conduct the tests in the present study was fabricated under the scope of the present project. This chapter includes a detailed description on the design and fabrication aspects associated with both the B_{ALT} and S_{ALT} procedures.

3.2 Beam Accelerated Load Testing, B_{ALT}

The B_{ALT} procedure has been developed with a vision to make the joint performance evaluation task very simple and economical so that the test can be conducted using readily available laboratory resources or with a marginal investment. In the B_{ALT} procedure, joint performance can be characterized by (i) using the conventional 24- x 6- x 6-in beam specimens that are actually cast for modulus of rupture testing, (ii) performing the test on a scaled down facility and (iii) using only one single low capacity (max. capacity ~2000 lbs) actuator. These objectives were achieved by (i) designing and fabricating the B_{ALT} in such a way that the mechanical action induced on the joints of an in-service concrete pavement can be replicated in the B_{ALT} procedure, (ii) determining magnitude of the scaled down load corresponding to an equivalent standard axle load (ESAL), (9000 lb), (iii) determining the location for the application of the scaled down load and (iv) establishing the specimen preparation, testing and data collection procedures.

3.2.1 Setup design principle

The test setup was design to replicate the abrasive action that occurs on the joints of an in-service concrete pavement. Both the conditions (i) when the wheel is on the approach (case I) and (ii) when the wheel is on the leave slab (case II) were considered. In the B_{ALT} procedure, unlike the in-service pavements, load is applied only on one side of the joint. In the in-service condition, when the load is applied on the approach slab, the approach slab directly deflects down, and the leave slab is indirectly pulled down by the approach slab because of the load transfer phenomenon. When the load is applied on the leave slab, the actions reverse. Figure 3-1 demonstrates the above mentioned scenarios along with their corresponding simulations in the B_{ALT} procedure. In case I, when the approach slab moves down, an upward shearing resistance is generated on the fractured face of the leave slab (Figure 3-1 (a)). This upward shearing resistance was attained by applying an upward force on the right half of the beam (Figure 3-1 (b)). During the application of the load, the entire length of the beam was held under a constant restrainment at the top and bottom. More details regarding the restraint are discussed in the following subsection. In case II, the direction of the shear resistance on the fractured face of the leave slab is downward (Figure 3-1 (c)). This downward shear force was simulated by a downward force on the right half of the beam (Figure 3-1 (d)). To simulate the repeated wheel loads for the in-service condition, loads were applied alternatively in upward and downward directions. The magnitudes of the loads in both the directions were kept similar.

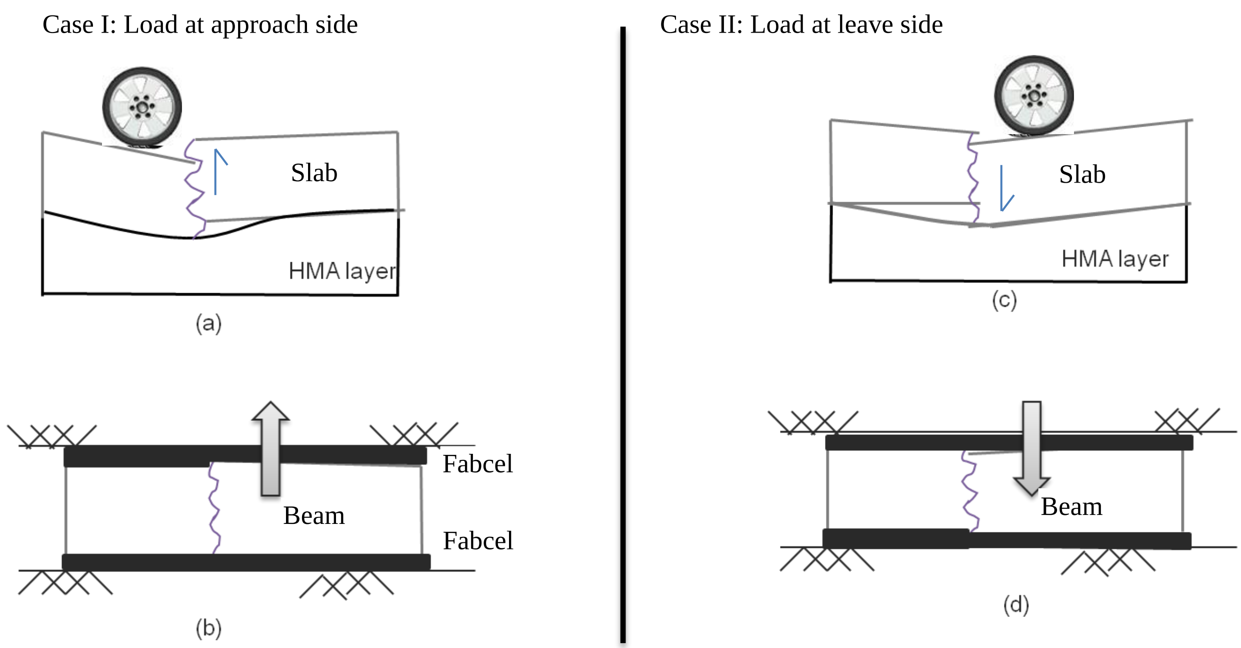

Figure 3-1: Loading scenarios in the in-service pavement and their simulation in the B_{ALT} procedure.

3.2.2 Components

Foundation and restraint: The foundation support provided by the lower layers under the concrete slab in an in-service pavement was replicated by an artificial foundation. Since, the load was applied in both upward and downward direction, an artificial foundation was provided at both the top and bottom of the specimen. Two layers of neoprene pads, known as Fabcel 25 (http://www.fabreeka.com/Products &productId=24), were used as the foundation. Figure 3-2 shows the picture of a Fabcel 25 waffle shaped neoprene pads.

The stiffness of the two combined Fabcel layers was determined by conducting plate load testing according to ASTM-D1195/D1195M, 2009), and was found as 200 psi/in. The specimen and Fabcel layers were vertically restrained so that the deflection under the load is only due to the compression of the Fabcel layers. Figure 3-3 shows a picture of the B_{ALT} setup. Figure 3-4 shows the cross section of the test setup. Different components can be seen in these two figures.

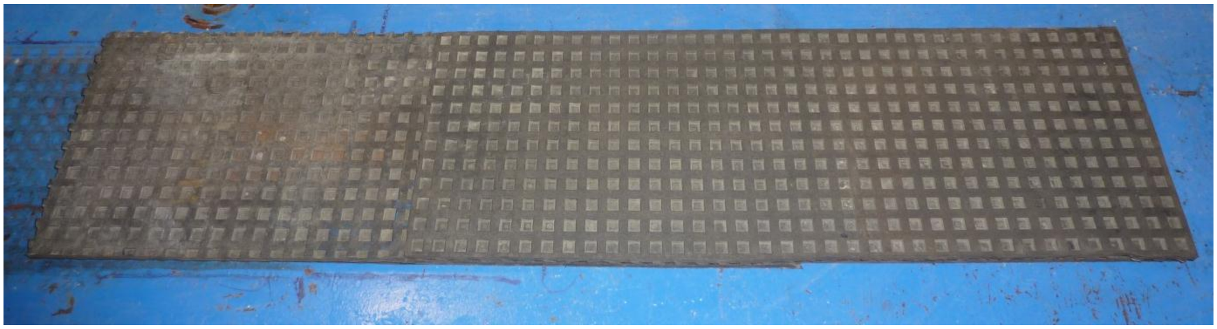

Figure 3-2: Picture of a waffle shape neoprene pad, Fabcel 25.

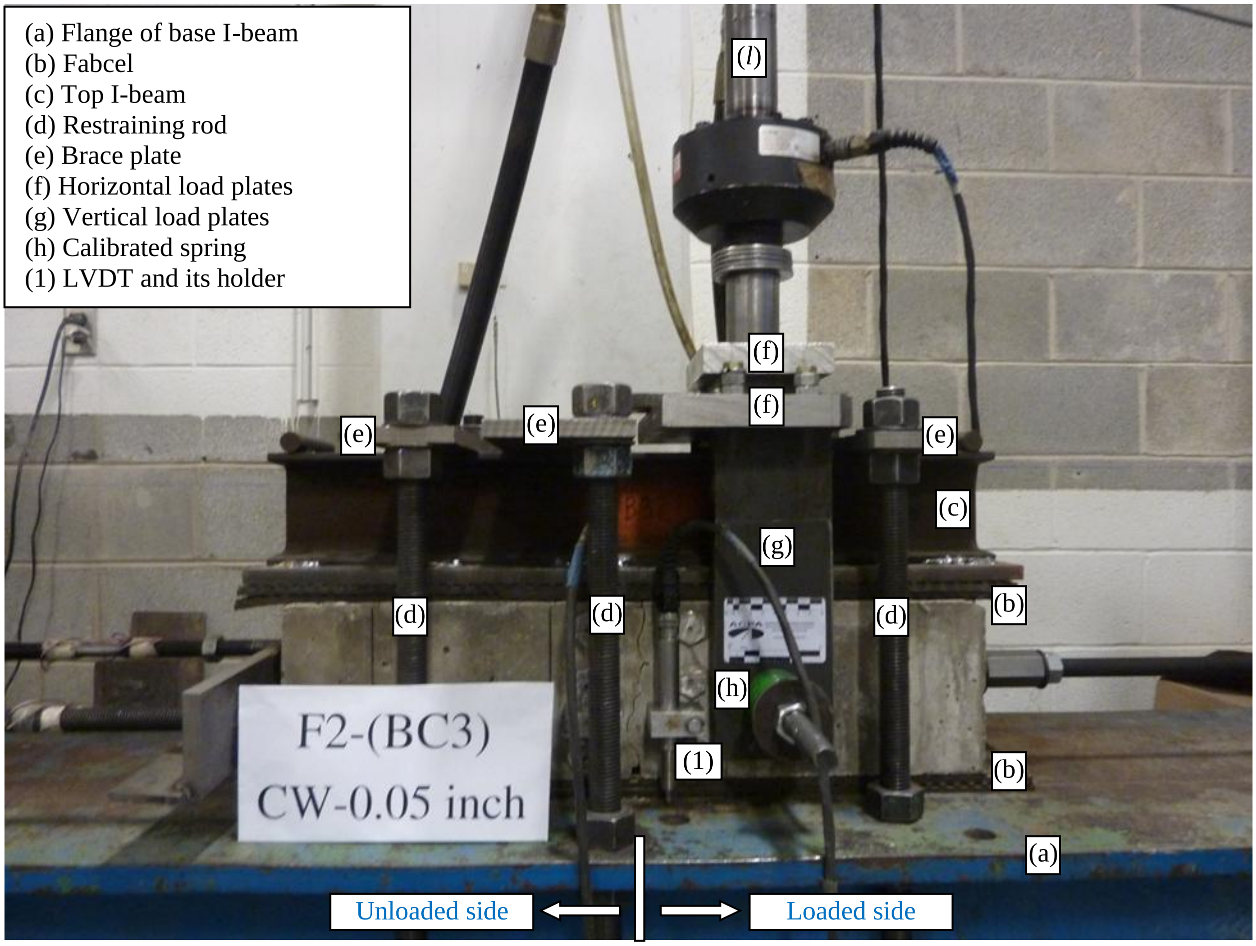

Figure 3-3: Photo of the B_{ALT} test setup.

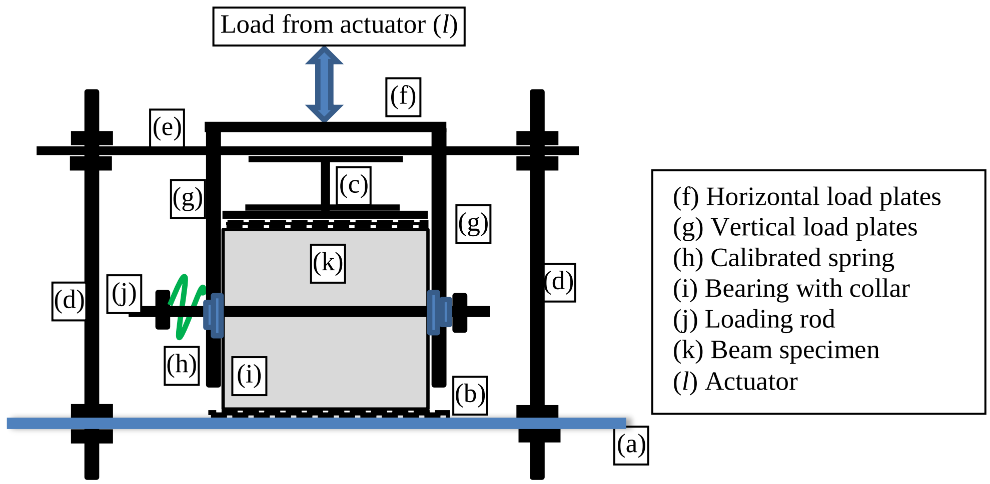

Figure 3-4: Schematic of the cross section of B_{ALT} setup.

A 17-inch wide I-beam, to be referred as the base I-beam in this study, was used as the platform for the B_{ALT} setup. This base I-beam was situated on the concrete floor of the lab. The Fabcel layers were directly laid on the top flange of this base I-beam. At the top of the specimen, a built up I-beam with a 6-in wide bottom flange (equal to the width of the beam specimen), was placed on the Fabcel layer. This I-beam is referred as the top I-beam in this study, and is shown in Figure 3-5.

To secure the top I-beam with the base I-beam, six 1-in diameter threaded rods (referred to as restraining rods), three brace plates and twenty four hexagonal nuts were used in the assembly. The test specimen, covered with two layers of Fabcel at top and bottom, rests in between top I-beam and base I-beam. The brace plates, which run across the top flange of the top I-beam, were strategically placed, one at the mid-span (on top of the joint) and the other two near the edges. These brace plates were secured with the top flange of the base I-beam by a pair of restraining rods. Hexagonal nuts were used to tight the assembly. A torque of 40 in-lb was applied to all the nuts located at the top of the brace plates that keep a uniform restraint along and across the specimen. It was observed that with a 40-in-lb torque, the reproducibility of the results (deflections and LTE) was better. The assembly was strong and sturdy with no or negligible movement of the top I-beam when the dynamic load was applied. A torque below 40 in-lb on the nuts provides higher deflection under tension loading, and a higher torque produces lower deflection in both the tension and compression loads. However, the torque on the nuts creates a pre-compression in the Fabcel layers. The deflections measured, with the help of linear variable differential transformer (LVDT), before and after the application of the torque, showed that the Fabcel layers compress by 25 mils under this level of applied torque.

Figure 3-5: The top I-beam in B_{ALT} setup.

Load application and deflection measurement arrangement: Load on the beam specimen was applied with the help of an actuator capable of applying load in both upward and downward directions. A special arrangement, as was shown in Figure 3-3 and Figure 3-4, has been developed to transfer the load from the actuator to the beam. Load was applied to the right half of the beam in the form of a shear force.

A horizontal load plate was connected with the actuator. This horizontal load plate distributes the load equally on two vertical load plates. The load from the vertical load plate to the beam is transferred through a specially designed bearing-collar assembly pressed fitted in each of the vertical load plates. See Figure 3-6. Each bearing has two collars attached, one at each side. The bearings transfer the load from the vertical load plates to the collars. The collar located at the inner face of each vertical load plate was partially projected out by 1/8 in. The projected surface of each inside collar was basically forced in surface to surface contact with the side walls of the beam, by a horizontal force. The horizontal force was applied through a ¾-in threaded rod, referred to as the loading rod. This rod runs through a calibrated spring, collars at the front vertical loading plate, a pre made horizontally aligned hole located at the mid-depth of the specimen and collars at the rear vertical loading plate. Nuts on this loading rod on each side of the beam are tightened to apply the horizontal force. The pictures of the calibrated spring, loading rod, nut, bearing and collar assembly are shown in Figure 3-6.

The load is quantified by the calibrated spring, which has a spring constant equal to 3000 lb/ in. The magnitude of the required horizontal tensile force at the loading rod or the compression at the collar-beam interface is a function of the load magnitude on each vertical load plate and coefficient of friction between the steel and concrete surfaces. Sufficient horizontal force was applied to generate the required frictional resistance at the collar-beam interface so that the total vertical load from the actuator was transferred to the beam, without any sliding. The magnitude and location of the load used is discussed in Section 3.2.3. The purpose of the bearings in the loading assembly was to create a hinge along the axis of the loading rod so that no moment is transferred to the beam either from the load or from the restrainment. The load induced deflection profile is therefore purely a function of the applied load magnitude, analogous to the in-service condition.

The deflections at both sides of the joint were measured by two LVDTs. One aluminum LVDT holder was glued on each side of the joint on the front side of the beam.

Crack width control arrangement: The crack width control assembly in the B_{ALT} setup can be seen in Figure 3-7 and Figure 3-8. Crack width was controlled by regulating a horizontal force along the length of the specimen. While casting the specimen, a ¾-in threaded rod is embedded in each end of the beam along the longitudinal axis. This rod is referred to as a tension rod. The embedded length of the tension rod was 4.5 in, while the exposed length was around 1.5 to 2 in. On the left hand side of the beam, the exposed end of the tension rod is connected to a horizontally aligned steel angle running across the width of the beam. Two more parallel ¾-in threaded rods (referred to as crack width (cw) control rods) coming out from this steel angle were connected to a vertical column through one more steel angel and a bracket, as shown in Figure 3-7.

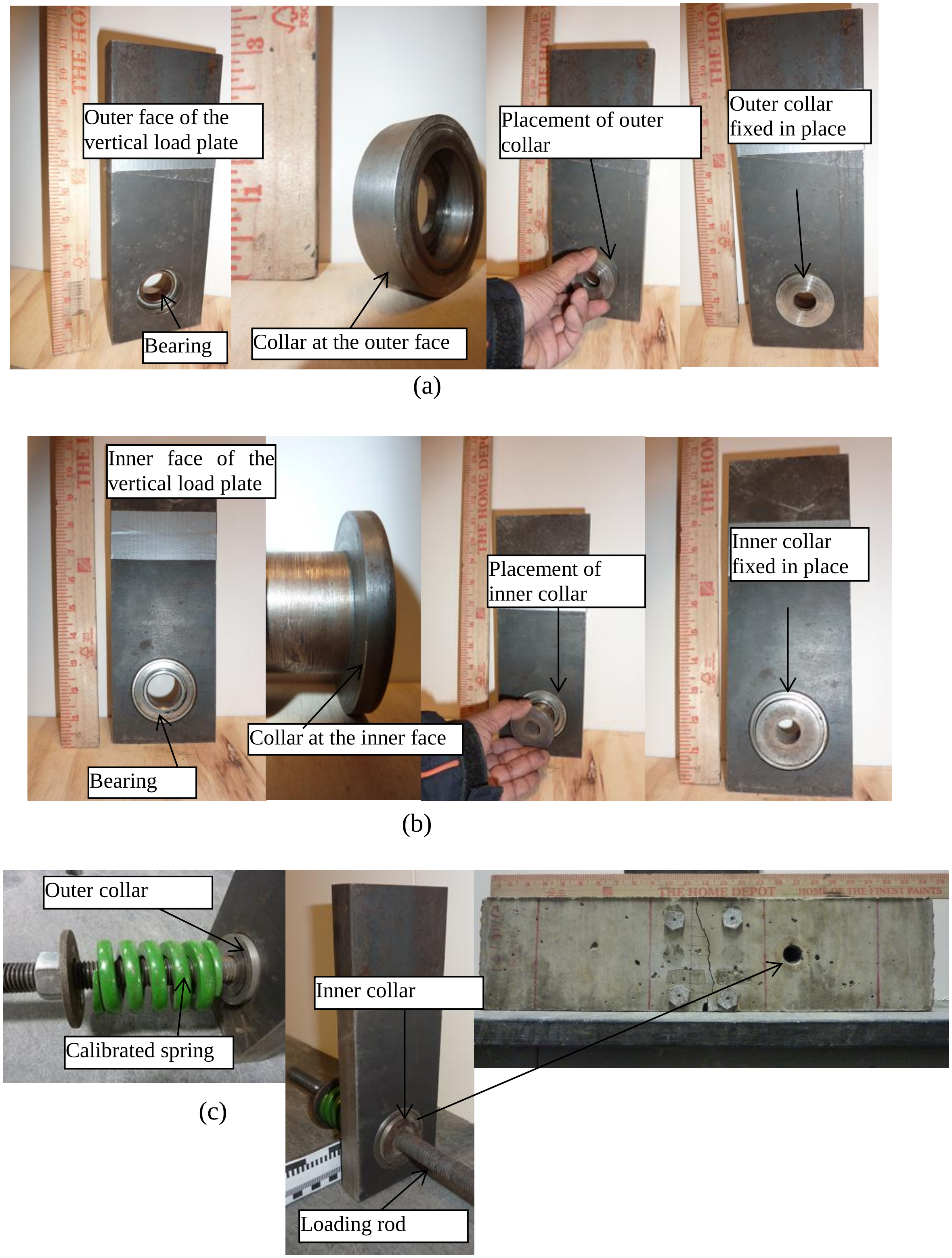

Figure 3-6: Loading and deflection measuring assembly (a) bearing and collar at the outer face of the vertical load plate (b) bearing and collar at the inner face of the vertical load plate (c) calibrated spring, loading rod and the concrete face where the inner collar remains in contact.

On the right hand side, the tension rod was lengthened with the help of a coupler. The right end of the extended rod was directly attached to the vertical column through a bracket. The horizontal force could be adjusted by tightening and loosening the hexagonal nuts on the tension rod at the left hand side. The purpose of having two cw control rods on the left hand side was to ensure an independent crack width tuning facility on either side (front and back) of the beam. Also, these rods could be moved up and down.

These arrangements helped to keep a uniform crack width throughout the cross section of the specimen. Sometime when fibers beams were tested, because of the non-uniform distribution of the fibers, a uniaxial horizontal force was unable to make a uniform crack width throughout the cross section. In this kind of situation, an extra moment was applied by adjusting the orientation of the cw control rods. This extra moment opens up the crack on the side where it was narrow when only a uniaxial horizontal force was applied. The right hand end was not disturbed during the test, partially because the actuator was connected to this side of the beam. A considerable movement of this end might misalign the actuator resulting in an oblique loading. The force on the cw control rods was measured using a strain gage attached to each cw control road. Threads on the cw control rods were locally machined off at the strain gage locations before they were mounted.

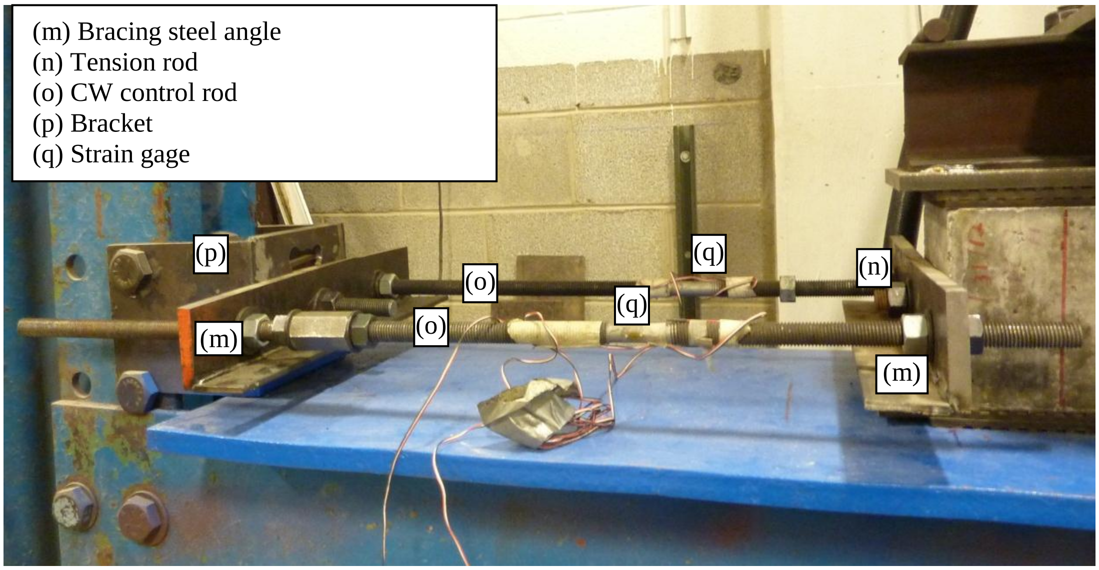

Figure 3-7: Crack width control assembly on the left hand side of the beam.

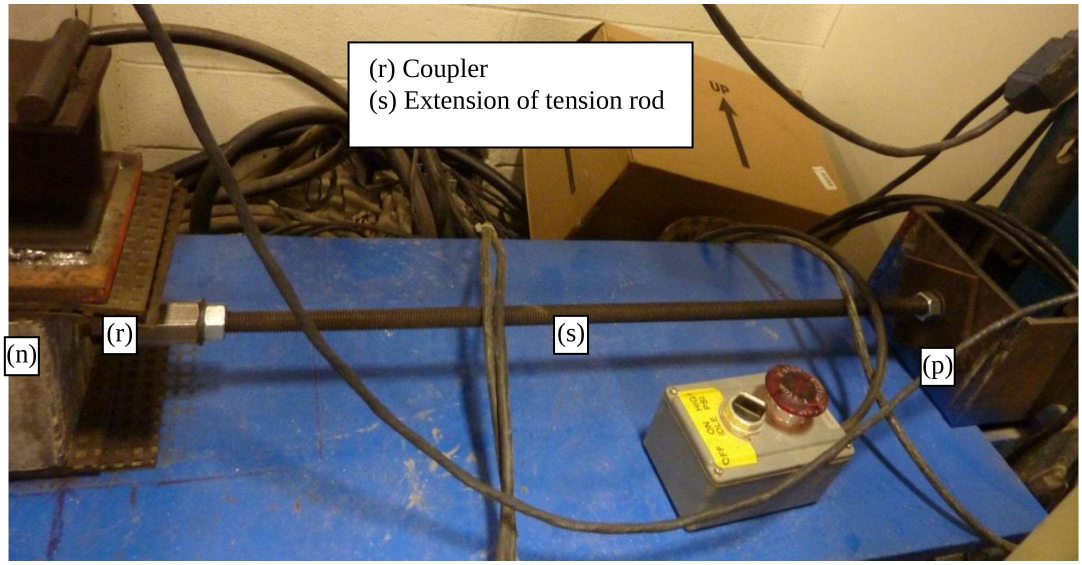

Figure 3-8: Crack width control assembly on the right hand side of the beam.

3.2.3 Load magnitude and location

The magnitude and location of the load in the B_{ALT} procedure were determined through an analysis using the finite element method (FEM). The finite element analysis software, ABAQUS FEA (http://www.3ds.com/products/simulia/portfolio/abaqus/overview/) was utilized. The B_{ALT} procedure was modeled in such a manner to capture the equivalent joint performance between the two adjacent 4-in thick, 5-ft x 6-ft whitetopping slabs. First a FEM model for the above mentioned slab was developed. Then, using similar material properties, a model for the beam specimen was developed. Deflection profiles for the 12- in x 6-in x 6-in beam specimen (half of a 24-in long beam) in the B_{ALT} procedure were matched with the deflection profiles for the 4-in slab in the S_{ALT} procedure. A detail of the modeling features for both the procedures is described below.

Table 1 presents the general features for the slab model. Figure 3-9 shows a screenshot of the slab model in ABAQUS. A load of 9000 lbs was applied on a space 10- x 10-in square area on the right hand side of the slab. The center of the loading area is 18 in away from the left hand side longitudinal edge and 6 in away from the transverse joint, analogous to the Raja & Snyder, 1995 study. Both the adjacent slabs are rested on an elastic foundation with a stiffness equivalent to 200 psi/inch modulus of subgrade reaction. Two layers of Fabcel-25 pads provide such foundation stiffness. The load transfer between the adjacent slabs was modeled using translational springs in the Z- direction. Each pair of nodes on the adjacent slab across the transverse and longitudinal joints was connected by one single spring.

Table 1: Input and FEM modeling features for the concrete slab model.

Slab size	60 x 72 x 4 inch
Modulus of elasticity of concrete	4,000,000 psi
Poisson's ratio of concrete	0.15
Density of concrete	0.0026 slugs/inch^3
Modulus of subgrade reaction	200 psi/in
Element type	27 noded brick
Element size	1 x 1 x 1 inch

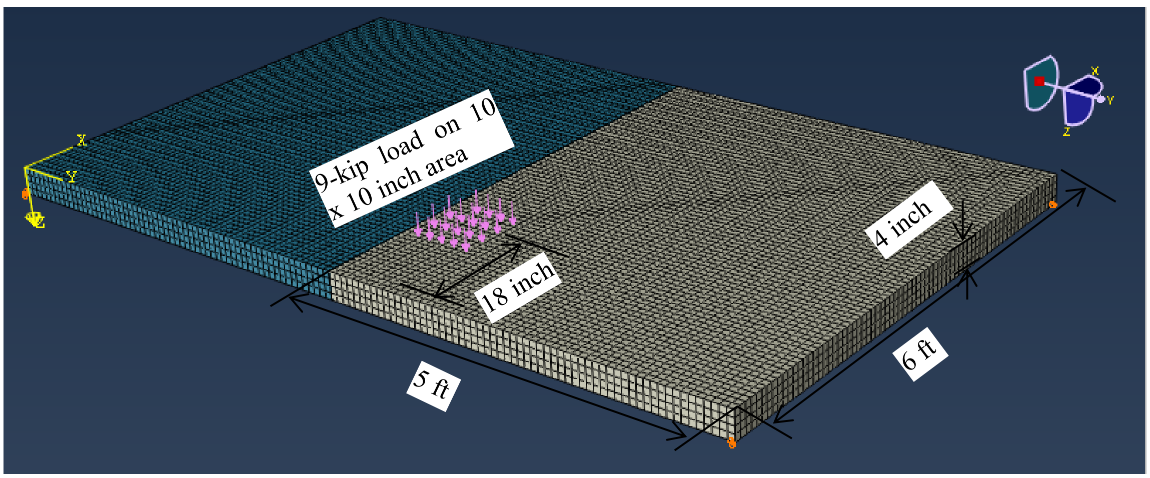

Figure 3-9: Screenshot of the slab model.

The joint stiffness (*AGG*) is a spring constant that relates to the non-dimensional joint stiffness (*AGG*= AGG/kl).* Using the Ioannides & Korovesis, 1990 relationship for the LTE vs *AGG**, *AGG** for a given LTE can be determined. The stiffness assigned to each node, K, is based on the area contributing to the stiffness of that node. The ratio of the areas covered by the corner, edge and intermediate nodes is 1:2:4, therefore, for equally spaced nodes the spring constants can also be assigned in that ratio. The following equations (3-1), (3-2) and (3-3) (Feng & Ming, 2009) are used to determine the respective spring constants assuming uniformly spaced nodes.

$$K_{corner} = \frac{kLlAGG^*}{4(N_r - 1)(N_c - 1)} \quad (3\text{-}1)$$

$$K_{edge} = 2K_{corner} \tag{3-2}$$

$$K_{intermediate} = 4K_{corner} \tag{3-3}$$

where K_{corner}, K_{edge} and $K_{intermediate}$ are the spring constants (lb/in) at the corner, edge and intermediate nodes on the joint faces, respectively; k is the modulus of subgrade reaction (psi/inch); L is the width of the slab (inch), 72 inch in the present case; l is the radius of relative stiffness (inch); $AGG*$ is the non-dimensional joint stiffness; N_r and $N_c$and are the numbers of rows and columns of nodes on the joint face, which depend on the element size, type and area of the cross section of the slab.

Using the slab model, deflection profiles were generated for two different cases, one with an 85 percent LTE and the other with a 90 percent LTE. Relatively higher LTEs were chosen so that the influence of the joint performance is dominant in the generated deflection profiles, but not the foundation. The deflection profiles for the two cases are shown in Figure 3-10 and Figure 3-11. The maximum deflections obtained for the two cases are quite similar, 0.034 and 0.033 inches for 85 and 90 percent LTEs, respectively. The slope of the generated deflection profiles, calculated for a12-in length starting from the transverse joint, were -1/1350 and -1/1430 at 85 and 90 percent LTEs, respectively. The slopes on the loaded side of the slab were considered. The reason for determining the slope only up to a 12- in length is because the length of loaded side of specimen in the B_{ALT} procedure is also 12 in.

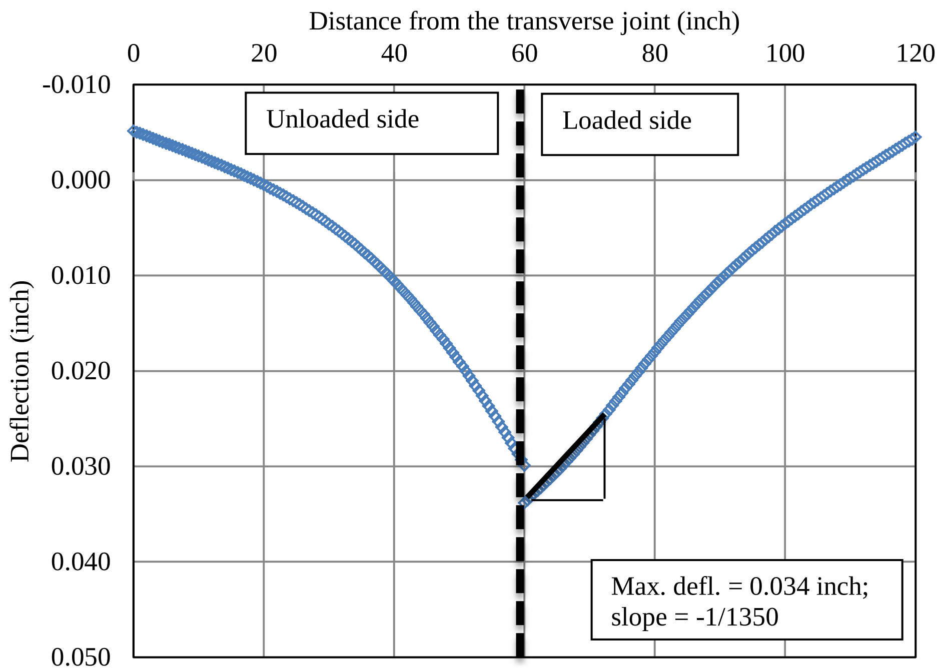

Figure 3-10: Deflection profile of slab at 85% LTE.

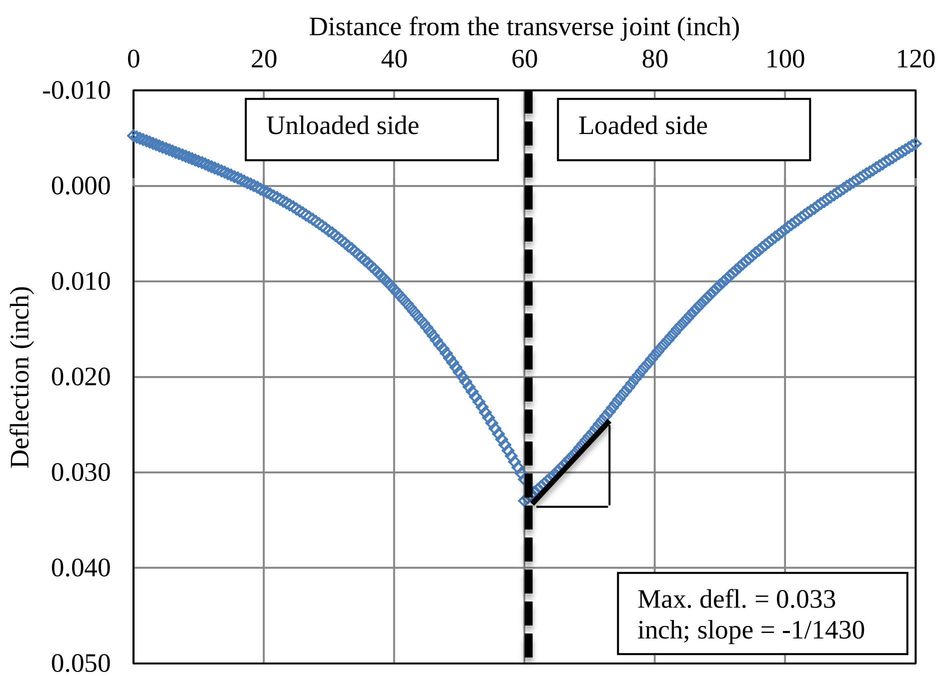

Figure 3-11: Deflection profile of slab at 90% LTE.

Next, the beam model was developed. The input related to foundation, materials and modeling features were kept similar to that of the slab model, as was given in Table 1. The load in the beam model was applied in the form of surface traction on a 6 in^2 rectangular area, on both the front and back side walls. This loading scenario was chosen to simulate the applied force in the B_{ALT}. Figure 3-12 presents a screenshot of the beam model with the loading area shown at the front side of the beam. The ratio of the joint spring constants (K_{corner}, K_{edge} and $K_{intermediate}$) was 1:2:4. Figure 3-13 shows the transverse joint springs in the beam model and the modeled elastic foundation.

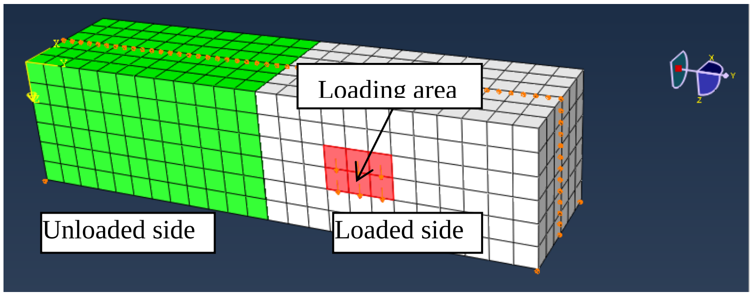

Figure 3-12: Beam model with the loading area depicted.

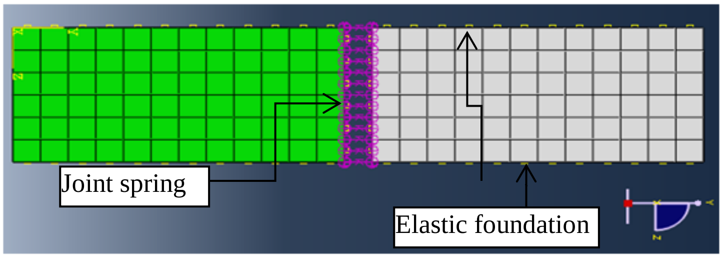

Figure 3-13: Side view of the beam model showing joint springs and foundations.

It was desired that the deflection and rotation of the beam simulated that of the slab. The load magnitude and location were selected to achieve these goals. Both the slab from the S_{ALT} and beam from the B_{ALT} were analyzed using the FEM so the deflection and rotation could be characterized for a range of load magnitudes and load locations. The analysis was performed for LTE of 85 and 90 percent. The generated deflection profiles for the beam were compared with deflection profiles for the slab (Figure 3-10 and Figure 3-11). An initial scanning of the beam deflections revealed that the magnitude of the load in the beam could be within the range of 1000 to 1100 lbs and the location between 4 to 5 in. Table 2 presents the values of maximum deflections and the slope of deflection profiles for a few of the runs which were found to be closer to the slab deflection profiles at 85 and 90 percent LTEs. Figure 3-14 and Figure 3-15 provide the graphical comparison of the deflection profiles. It can be seen that in both cases (85 and 90 percent LTE) the maximum deflection and slope for the beam closely matches with the slab when the load magnitude and location are 1050 lbs and 4.5 in, respectively. Hence, the magnitude and location of the load in the beam test was selected as 1050 lbs and 4.5 in.

Table 2: Maximum deflection and the deflection profile slope for different load magnitude and locations.

Target LTE (%)	Load (lb)	Dist. from the trans. joint (in)	Maximum deflection (in)	Slope
85	1000	4.0	0.038	-1/543
85	1000	4.5	0.033	-1/1124
85	1000	5.0	0.028	1/155584
85	1050	4.5	0.035	-1/1070
85	1100	4.0	0.042	-1/495
85	1100	4.5	0.036	-1/1026
85	1100	5.0	0.031	1/14286
90	1000	4.0	0.036	-1/604
90	1000	4.5	0.032	-1/1379
90	1000	5.0	0.027	1/4881
90	1050	4.5	0.033	-1/1313
90	1100	4.0	0.040	-1/550
90	1100	4.5	0.035	-1/1253

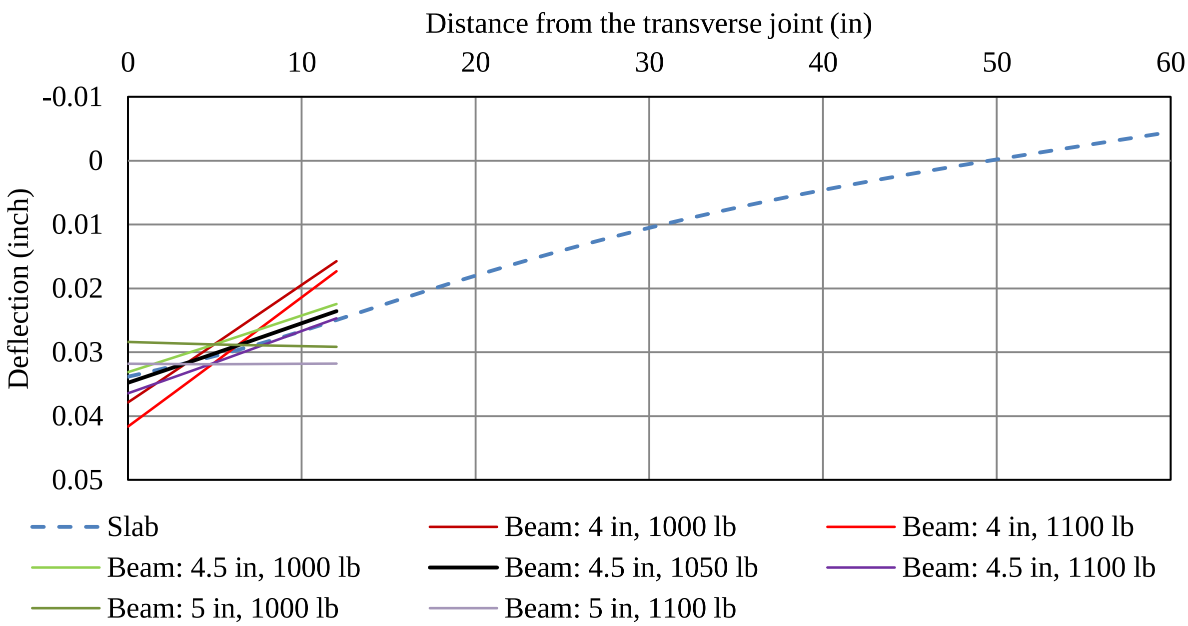

Figure 3-14: Comparison of the deflection profiles for the beam and slab at 85 percent LTE.

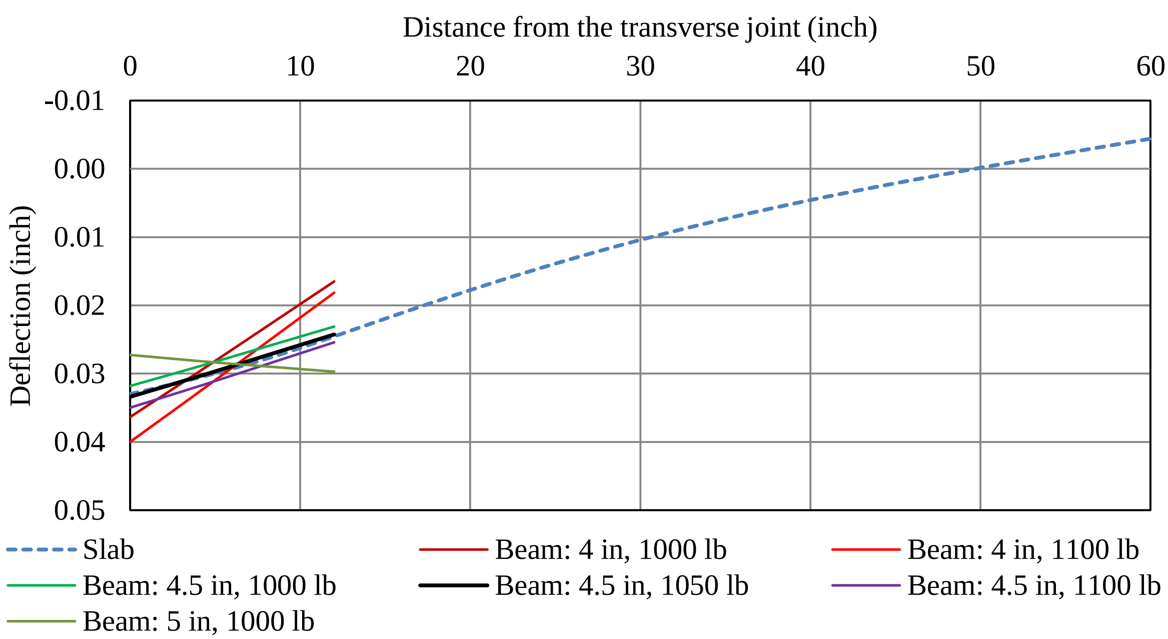

Figure 3-15: Comparison of the deflection profiles for the beam and slab at 90 percent LTE.

3.2.4 Specimen preparation

One of the advantages of the B_{ALT} procedure is the utilization of the readily available 24- x 6- x 6-in steel beam molds for specimen preparation. These molds are generally utilized to make beams for modulus of rupture testing of concrete (ASTM-C78/C78M, 2010). Test specimens were prepared in a manner such that the specimen has one tension rod at each end along the longitudinal axis, and has a notched crack at the bottom at mid-span controlling the location of the fracture plane. In the present study, 24- x 6- x 6-in steel mold was used with some modification. To accommodate the tension rod at both the ends, the steel end caps were replaced with wooden planks, as shown in Figure 3-16. The wooden planks were pressed fitted at the end of the longitudinal sides using the bolts available at the end of each longitudinal side. Holes were drilled through the center to accommodate the tension rods. A steel wire was looped around the all four sides to provide an extra rigidity so that the end caps were held securely in place. Nuts were firmly tightened on both sides of the plank to secure the tension rods firmly in place. A ½- x ¼- x 6- in metal bar was glued at the center of the bottom plate to create a notch for crack initiation. A horizontally aligned hollow PVC pipe was attached in the mold to keep the space for the loading rod. Two plastic end caps were glued to the surface of the longitudinal walls of the mold to hold the pipe horizontal. The inside diameter of the pipe was ¾ in. The pipe was placed in a location such that the longitudinal axis of the pipe was 4.5 in away from the mid-span of the beam and 3 in above the bottom plate.

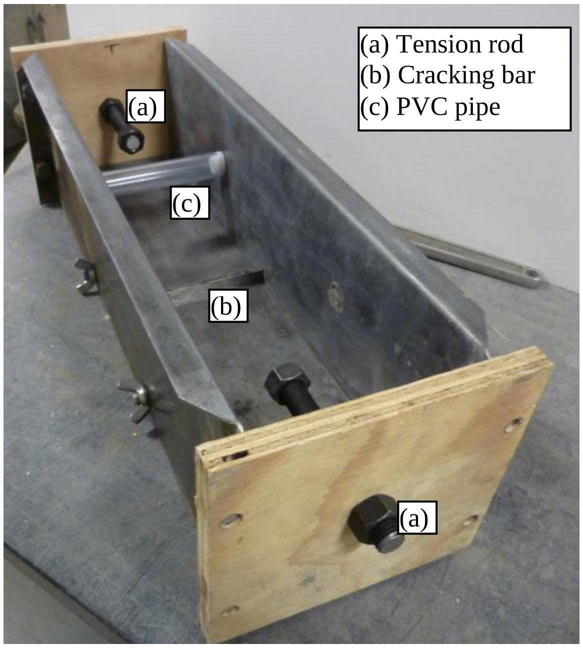

Figure 3-16: B_{ALT} test specimen mold.

The specimens were cast in accordance with ASTM-C1609/D1609M, 2010 and ASTM-C78/C78M, 2010. Extra care was required to keep the crack initiation bar and PVC pipe in place during the casting. The concrete was placed in two layers with the required vibration in each layer by obtained with table vibrator. Most of the time, a temping rod was used at the corners in addition to the vibration to avoid any honey combing. Figure 3-17 shows one example of a FRC beam preparation.

Figure 3-17: Preparation of an FRC beam specimen is in progress.

Specimens were demolded at 14 to 15 hours after casting. The crack initiation bar and the plastic end caps attached to the PVC pipe, were removed. A gentle tapping with a screw driver on one end of the crack initiation bar slides it out easily, as shown in Figure 3-18. The next task was to adhere three pairs of aluminum gage studs on each side of the specimen, as shown in Figure 3-19. These studs had a conical shaped slot on them. The distance between the slots in each pair of studs was measured in triplicate when recording the initial gage distance. The purpose of the gage studs was to monitor the crack width.

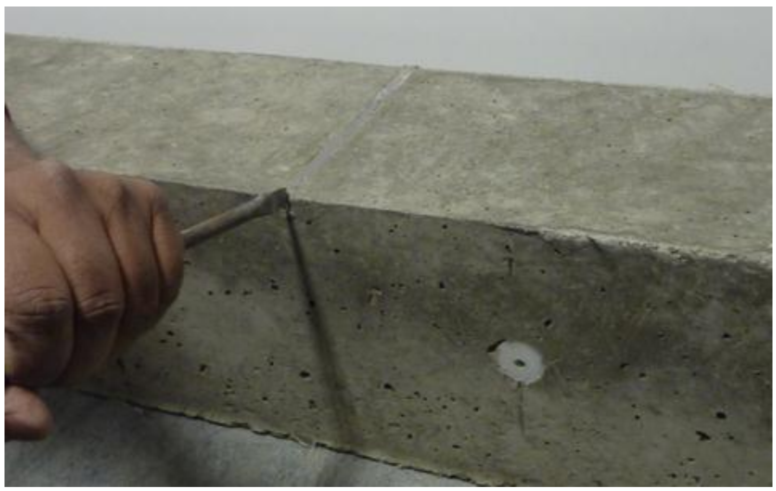

Figure 3-18: Removal of cracking bar from the concrete.

At 18 hours, the specimen was cracked at mid-span by applying a flexural load in the same manner used for a MOR test. Figure 3-20 shows cracking of an FRC beam. The loading rate, 15 to 45 lb/sec, was kept constant during the cracking process in accordance with ASTM-C78/C78M, 2010. During the cracking procedure, extra attention is required to ensure the beam is unloaded immediately after crack development. Initiation of the crack or just development of a very tight crack should be considered sufficient. Therefore, loading was stopped just after the appearance of a crack on the concrete surface. This is difficult to achieve for beams without fibers. Putting the two separated halves of the beam back exactly in the same position, matching the crack surface textures, is really a challenging task. In the FRC beams, fibers bridge the crack, so the beam halves do not generally fall apart. See in Figure 3-21. One notable point in this procedure of cracking is that the crack width at the bottom becomes wider than the top. This also simulates the non-uniform crack width pattern of an in-service pavement condition. In the present work, the cracked beams were transferred on a wooden plank right after the cracking procedure. Further handling of specimens were performed on the plank so that the crack faces remain undisturbed until they were placed in the test setup. The cracked beams were cured for 28 days in a moist curing room at a relative humidity greater than 100 percent.

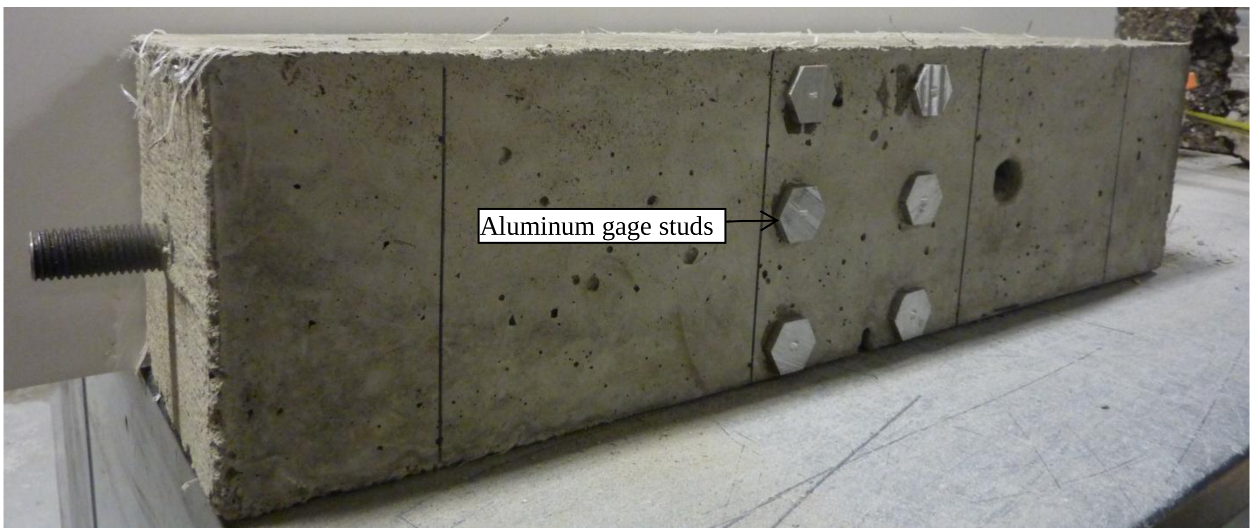

Figure 3-19: Aluminum gage studs for measuring crack width.

Figure 3-20: Cracking procedure for the beams used for B_{ALT}.

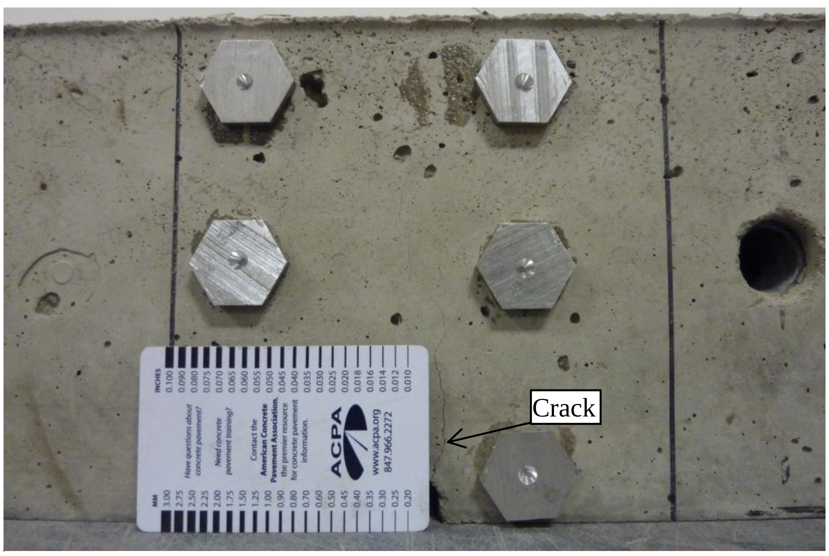

Figure 3-21: An FRC beam cracked at 18 hours.

3.2.5 Test Procedure

Now that a description of how the B_{ALT} specimen is prepared has been provided, a description of the B_{ALT} test will be provided. Before testing begins, the top surface of it must be inspected to verify the surface is smooth. If considerable undulation or irregularity is present on the beam surface, the surface is ground to obtain a smoother level surface. After the surface is checked, the beam is carefully placed on the lower layer of Fabcel. The top Fabcel layers and the top I-beam are then placed on top of the beam. Care must be taken when handling the beam so the crack width is maintained. The restraining rods, bracing plates and the crack width control assembly are then set in place. The beam on the frame was positioned with care so that that the axis of the vertically aligned actuator is directly above the loading location. Then, the loading components such as loading rod, vertical load plates assembled with bearing and collars, and the calibrated spring are put in their respective place, as discussed in the Subsection 3.2.2. After that, the nuts on the restraint rods are tightened. The nuts on the bracing plates are tightened with a 40- in-lb torque. Then, while holding the vertical load plates aligned, the actuator in which the horizontal load plate is already attached is brought down in contact with the vertical load plates. A very minimal load, such as 5 to 10 lbs, is applied during this process so that the vertical plates come in contact with the horizontal load plate attached to the actuator. The horizontal force is then applied. The magnitude of the horizontal force is estimated based on the load on each vertical load plate, area of the surface of each inner collar that remains in contact with the concrete and coefficient of friction between the concrete and steel surfaces. The estimated horizontal force, which was 1500 lbs, was ensured by attaining a half in reduction in the length of the calibrated spring. The spring constant of the calibrated spring was 3000 lbs/ in. The vertical load plates were tightly fastened with the horizontal load plate by bolts.

Once the beam was successfully placed in the loading assembly, two LVDT holders were glued with epoxy to the vertical walls of the beam at front side. These holders were placed such that the deflections could be measured 1 in distance from crack on both sides of the crack. LVDTs were then mounted in the holders. Next, depending on the existing crack condition, the desired initial crack width was obtained using the cw control assembly. In the case of the plain concrete beams, obtaining the desired uniform initial crack width on all four sides of the beam was relatively easy as compared to FRC beams. Force and moment were applied through the tension rods to stabilize a uniform crack width, as previously discussed in Subsection 3.2.2. Also, a low magnitude, dynamic, vertical load (300 to 500 lb) with a low frequency (2 to 4 Hz) was sometimes applied in addition to the horizontal force through the tension rod, especially in the case of FRC beams. An average of the crack widths measured at the 3 locations (top, middle and bottom) on each side of the beam was used to establish considered as the crack width of the joint.

Finally, when the setup was completely ready, a sinusoidal load cycle was applied through the actuator to obtain the load and deflection profiles. The magnitude of the peak load was 1050 lbs in both upward and downward directions. The loading frequency was 10 Hz. The typical load and deflection profiles are discussed in Section 3.4.1. The joint performance in the present study was evaluated at different crack widths and at different load cycles. The joint performance estimation procedures will be discussed in Section 3.4.

3.3 Slab Accelerated Load Testing, S_{ALT}

The large-scale test setup was developed to perform the joint performance test on real size slabs. The developed setup simulates the impact of a passing wheel on the transverse joints between two adjacent slabs. This setup is capable of testing slabs with millions of load cycles in a relatively short period of time. The main purpose of the S_{ALT} was to investigate the validity of the joint performance results obtain with the B_{ALT} procedure. The following subsections briefly describe the details of the S_{ALT} setup.

3.3.1 Setup design principle

The S_{ALT} setup in the present study was developed in a similar manner to the setup developed in Raja & Snyder, 1995 study. The vehicle load was simulated using two actuators. These actuators provide sinusoidal loads on both sides of the joint. The peak loads on the approach and leave slabs were applied with a phase difference. The phase angle is established based on the desired vehicle speed.

3.3.2 Components

Foundation: A concrete foundation, 12-ft long, 6-ft width and 2.75-ft deep, was used as the test platform. This was cast on a concrete reaction floor. Figure 3-22 shows a picture of the form work built to cast the foundation. Concrete was poured in three separate and equal layers. To strengthen the foundation at the mid-span, where the actuators would apply load during the joint performance test, a steel I-beam was embedded, as shown in Figure 3-22. Figure 3-23 presents a picture of the test setup showing platform for the S_{ALT}.

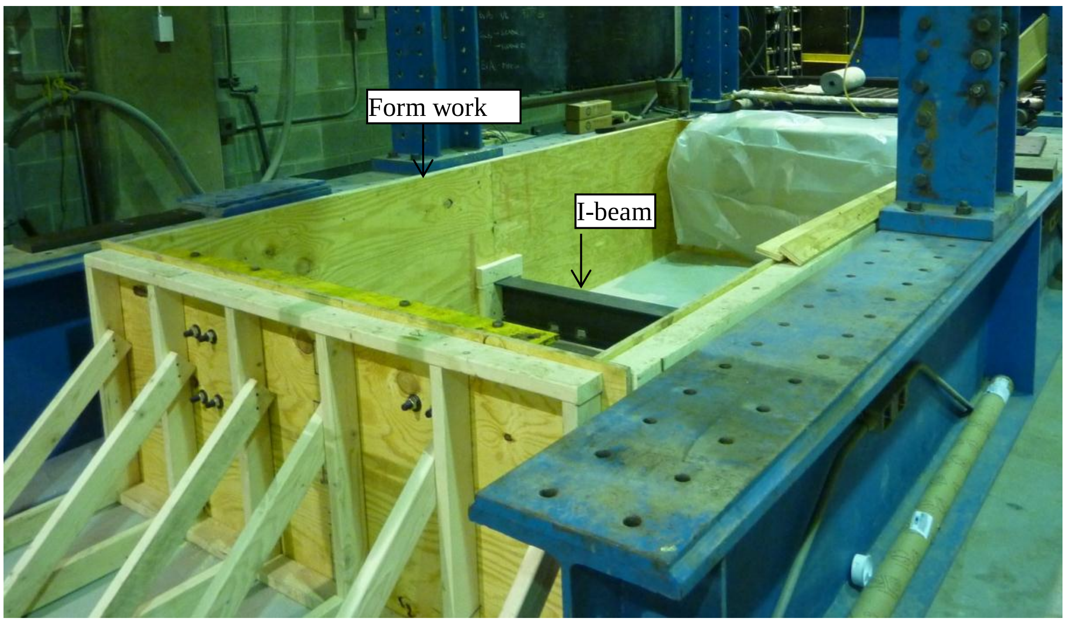

Figure 3-22: The form work used to cast the foundation.

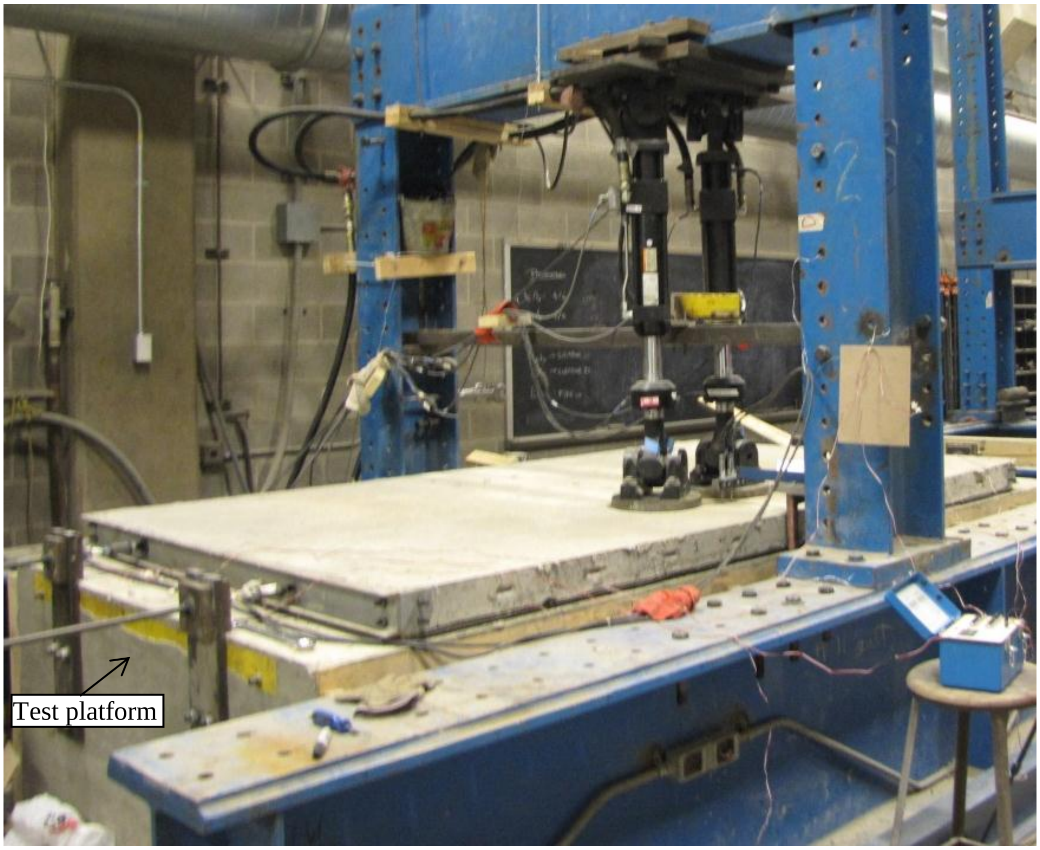

Figure 3-23: S_{ALT} setup.

As similar to the B_{ALT} setup, two layers of Fabcel 25 were used to simulate the subgrade with a modulus of subgrade reaction equal to 200 psi/in. Figure 3-24 presents a picture showing the two layers of Fabcel on top of the concrete foundation. Continuous vertical joints through the two Fabcel layers were avoided. Also, it was ensured that no joints between the pads coincide with the transverse joint of the test slab specimen.

Figure 3-24: Two layers of Fabcel 25 laid on the concrete foundation.

Test specimen

Different slabs sizes can be accommodated with this loading frame. In this study, 10-ft x 6-ft slabs, 4-in thick, were cast with a transverse crack initiated at the mid span (5-ft)

Casting frame

An example of the frames used to cast the slab is shown in Figure 3-25. Four inch deep steel channel sections were utilized for building the casting frame. The transverse sides were made with a single channel section whereas, the longitudinal sides are comprised of two separate channel sections, held together by a splice. See Figure 3-26. The longitudinal sides were tied by four equally spaced pencil rods which helped to attain a good rigidity in the transverse direction. Four I-bolts are placed on the two longitudinal sides of the frame so the crane can be used for lifting the specimen. See Figure 3-26. The other important components of the frame are the 26 shear keys. These are 2-in long steel rods welded on the inner side of the frame at an approximately equal spacing. These shear keys hold the slab from dropping out when it is lifted.

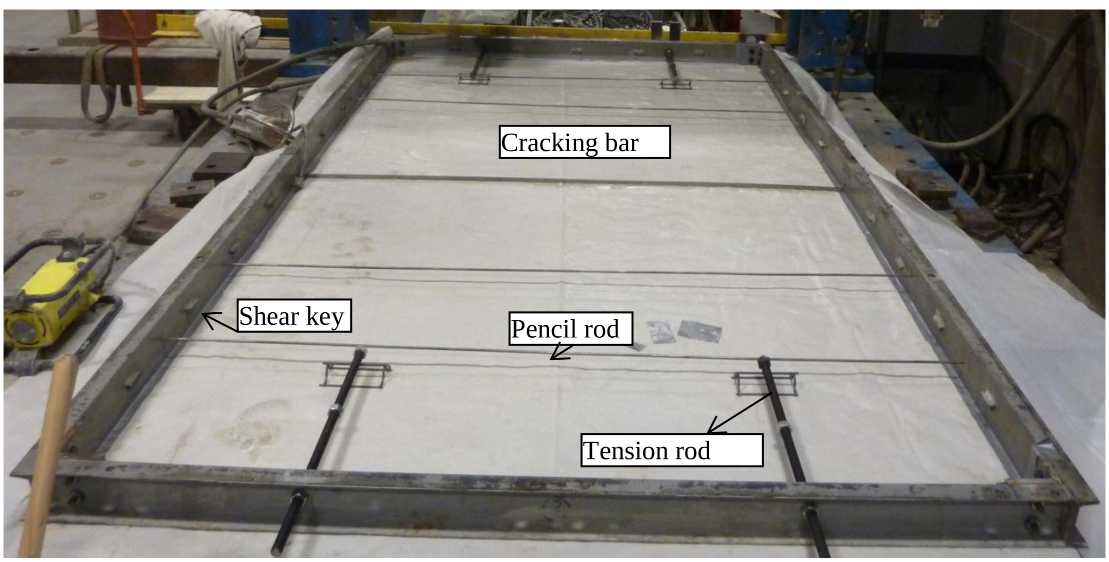

Figure 3-25: Test specimen frames for S_{ALT}.

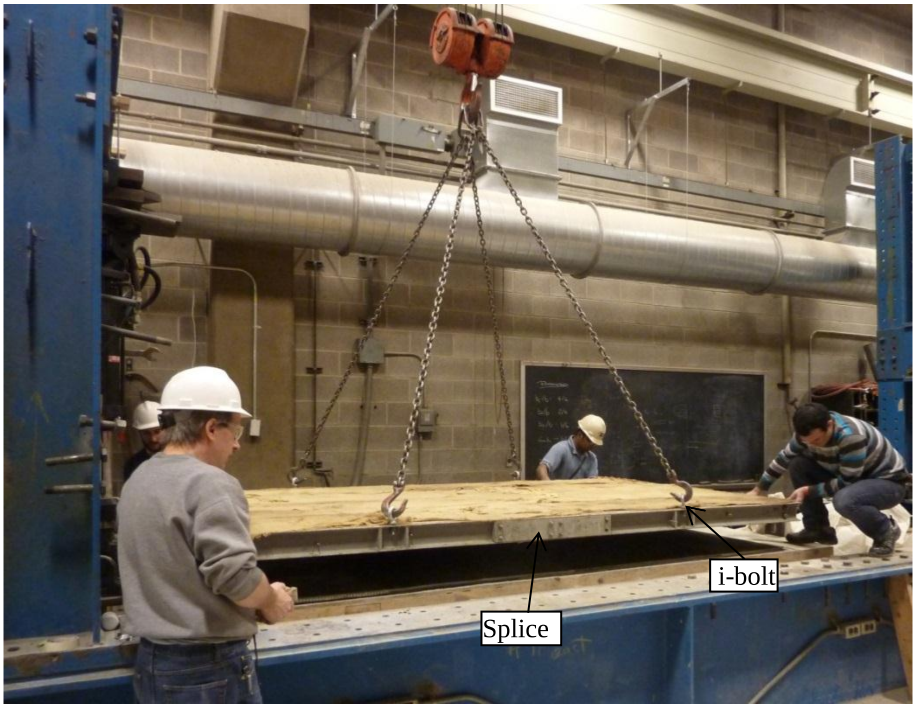

Figure 3-26: Slab is being placed after laying the Fabcel layers.

Crack width control assembly

Similar to the B_{ALT}, a crack width control assembly is also required in the S_{ALT}. While casting the slabs, four threaded rods, to be referred to as tension rods, with three hexagonal nuts on each of them, were cast in the concrete in four locations, as was shown in Figure 3-25. The embedded and exposed length of the tension rods were 28 and 6 in, respectively. Each of the tension rods was extended by another threaded rod during the testing of the slab. This rod is referred to as cw rod. The cw rod is connected to the tension plate, as shown in Figure 3-27. Tension plates were mounted (vertically) on the transverse side of the foundation through bolts cast into the foundation. The tension plate has a rectangular slot at the top to allow the tension rod through it. The crack width was established by loosening and tightening the nuts on the cw rod. Two larger washers are also used on both sides of the tension plate. The strain on the tension rod was measured by using strain gages affixed to each of the cw rods.

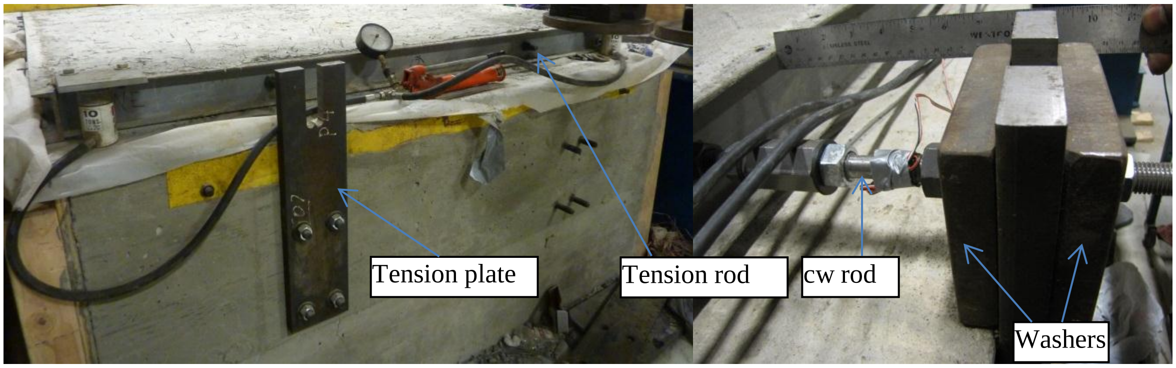

Figure 3-27: Crack width control assembly.

3.3.3 Specimen preparation

The slabs were cast on the foundation itself so that the bottom surface of the test specimen mimics the shape of the top surface of the foundation. This proved to be immensely helpful to avoid any gaps between the artificial foundation and test slab. It may be mentioned here that a couple of shakedown slabs were initially cast on the laboratory floor but when they were transferred to the foundation for testing, gaps were noticed in many locations. Therefore, all test slabs were cast on a plastic sheet on the foundation. A properly oiled ½- in x ¼-in x 6- ft steel bar, known as crack initiation bar was cast into the slab at mid span (Figure 3-25). This crack initiation bar created a weak zone, which helped in initiating the crack at the desired location at the bottom mid-span.

Casting of the slab generally started at mid-span (Figure 3-28). Shaft vibrators were used to consolidate the concrete. Figure 3-29 shows a photograph taken right after finishing the surface. Gage studs for crack width measurement were inserted into the concrete right after finishing the surface. A pair of gage studes are installed 3 in off the longitudinal edge on each side of the slab. The gage studs consisted of small bolts with a conical slot drilled into the head, as shown in Figure 3-30.

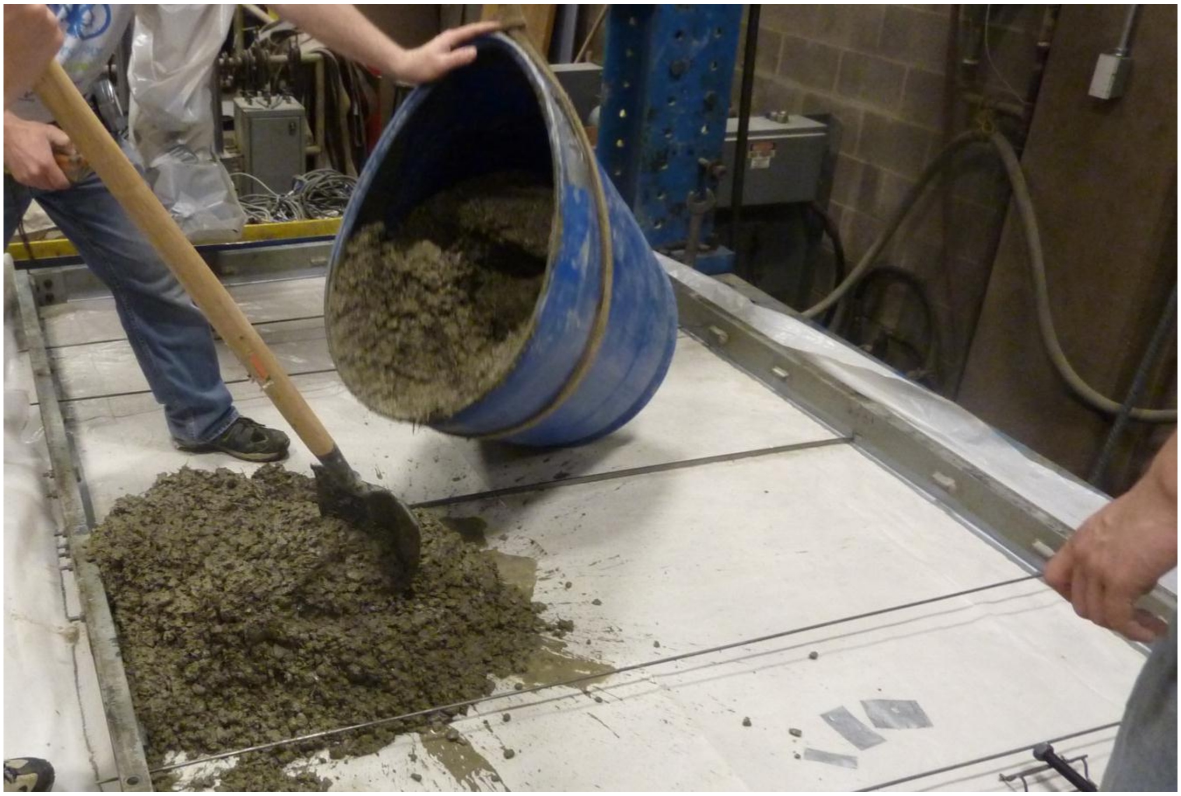

Figure 3-28: Casting of the slab.

Figure 3-29: Example of a finished slab.

Figure 3-30: Photograph of a pair gage studs inserted into the concrete.

The mid-slab transverse crack was initiated 18 hours after casting. A flexural load was applied to initiate the crack at the bottom of the slab and mid-span. One end of the 10-ft x 6-ft slab was jacked upward while restraining any upward movement on the other half of the slab. Figure 3-31 shows the slab cracking procedure. It can be seen that a 4-in x 4-in yellow steel angle was place at the middle of the slab. The angle was placed such that it rests on the restrained half of the 10-ft long slab, while the upward force was applied at the corners at the other end. The upward force was applied by using a pair of 10-ton hydraulic jacks through the two steel plates connected to the frame at the corners along the end. The slab was cured with plastic covered wet burlap for at least 28 days before testing.

Figure 3-31: Slab cracking procedure.

3.3.4 Test Procedure

Before loading of the slab can begin, the slab must be lifted off the foundation so that the Fabcel layers can be placed. The slab is then placed on top of the two layers of Fabcel. Proper referencing work was performed before moving the slab so that it could be replaced back in exactly on the same location from where it was lifted. After laying the Fabcel layers and setting the slab in place, the crack width control assembly was installed along with the deflection measuring assembly. The deflection measuring assembly consists of a 6-in wide steel plate attached to the concrete foundation, an arm connected to the steel plate, two aluminum LVDTs holder and two LVDTs. Figure 3-32 shows the two LVDTs mounted in the LVDT holders. Both of the LVDTs are placed 1in from the crack, one on the approach slab and the other one on the leave slab. Both are approximately 12 in from the longitudinal edge. The load was applied by two actuators through two 12-in diameter and 1-in thick circular load plates. A circular rubber pad was attached to each load plate to avoid any localized stress concentration on the slab. The location of the load plates and the LVDTs can be seen in the schematic presented in Figure 3-33.

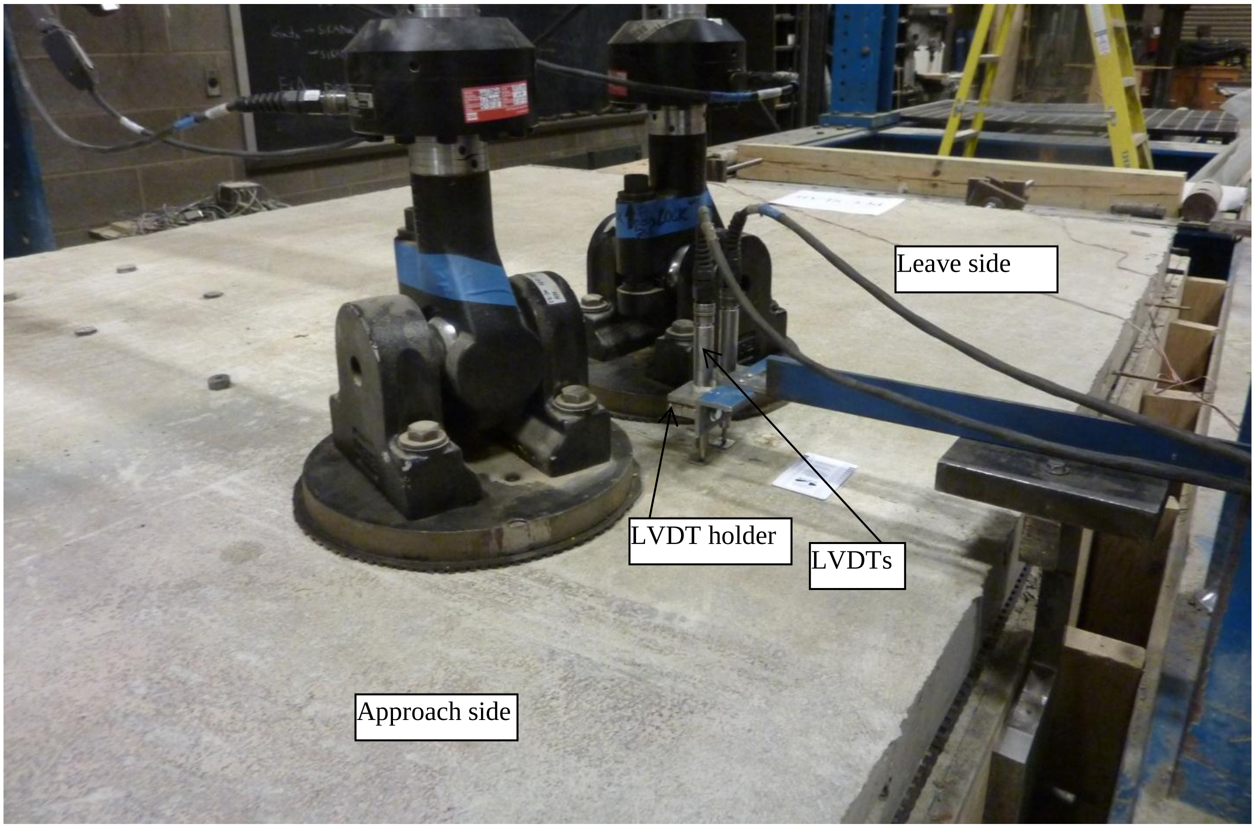

Figure 3-32: LVDTs and the LVDT holder for the S_{ALT}.

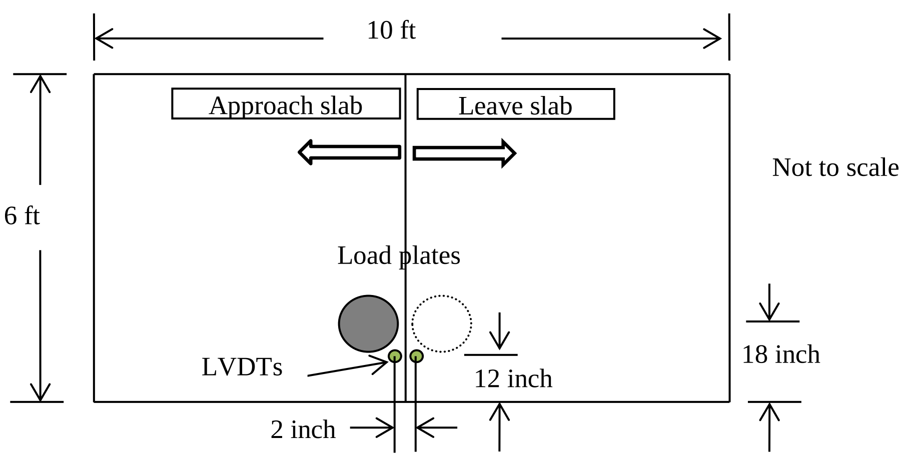

Figure 3-33: Location of load plates and LVDTs in S_{ALT} procedure.

The joint performance test was conducted by applying a composite sinusoidal load profile through each actuator. The load profile was designed in such a way that each slab was loaded for a period of 0.035 seconds with a 0.165 seconds rest period providing a time of 0.20 seconds to complete each cycle. Thus, the overall load cycle frequency is 5 Hz. During the actual loading period, the load rises from 500 to 9000 lbs in each actuator. In the rest period, a 500-lb load was maintained so that the actuator and slab remain in contact. The two actuators were operated with a 90-degree phase difference. The time difference between the two peaks was 0.032 seconds, which was equivalent to a vehicle speed 30 to 35 mph. It was also ensured that when one actuator reaches its peak load, the other is applying the minimum 500-lb load. It may be noted that the magnitudes of the loading periods, rest periods, peak loads, loads at rest period and the phase difference between the peak loads of the two actuators may slightly vary with the joint condition. Similar to the B_{ALT}, the joint performance was evaluated at different crack widths and load applications. The joint performance evaluation concept followed in the S_{ALT} procedure is discussed in the next section.

3.4 Joint Performance Evaluation Procedure

The joint performance can be characterized in many ways, such as in terms of load transfer efficiency (LTE), differential deflection (DD), differential deflection ratio (DDR), differential energy dissipation (DED) and dissipated energy ratio (DER). In the present study, both the B_{ALT} and S_{ALT} procedures are able to produce any of the above mentioned joint performance characterization parameters. These parameters are derived either from the load and/or deflection profiles.

The following subsections describe the concepts of evaluating the joint performance through LTE and DER in both the B_{ALT} and S_{ALT} procedures.

3.4.1 Joint performance through LTE

B_{ALT}

The deflection load transfer efficiency, LTE, was obtained by using the deflections corresponding to the time of the peak loads. As was mentioned in the Subsection 3.2.2, load was applied in both upward and downward directions. Therefore, the LTE can be obtained in both the directions as well. The typical examples of the load and deflection profiles in the B_{ALT} procedure are shown in Figure 3-34. The negative sign represents the load and deflections in the upward direction when the actuator provides a tension load, whereas the positive sign represents the opposite. The presence of a very small phase difference between the peak load and peak deflection could be observed in Figure 3-34. This phase difference varies between 1 to 5 milliseconds and is a function of joint stiffness. This is due to the time dependent response of the Fabcel layers.

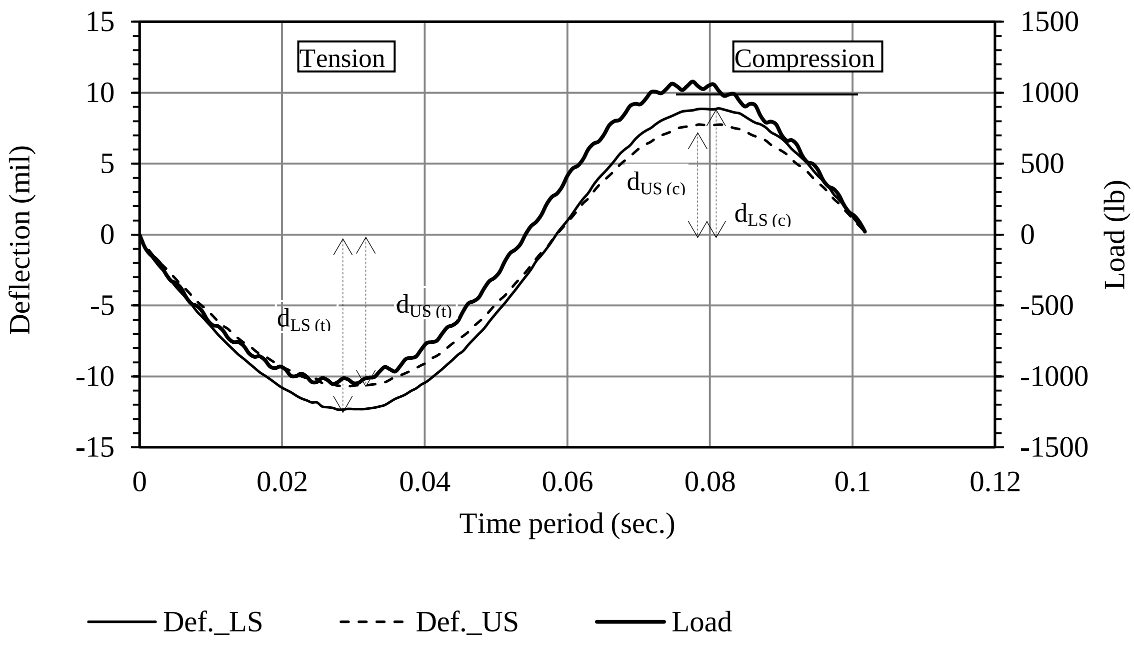

Figure 3-34: Load and deflection profiles for the B_{ALT}.

The LTE from B_{ALT}, LTE_B, is defined as the ratio of the unloaded side deflection to the loaded side deflection at the peak load. When the nature of the peak load is in tension, it is referred as the tension LTE, or $LTE_{B(t)}$, and when the nature of the load is compressive, it is referred as the compression LTE, or $\mathrm{LTE_{B(c)}}$. The LTE under both the tension and compression loads can be estimated by using the following equations.

$$\mathrm{LTE_{B(t)}} = \frac{d_{US(t)}}{d_{LS(t)}} \tag{3-4}$$

$$\mathrm{LTE_{B(c)}} = \frac{d_{US(c)}}{d_{LS(c)}} \tag{3-5}$$

where $d_{US(t)}$ and $d_{US(c)}$ are the unloaded side deflections under the tension and compression load, respectively; $d_{LS(t)}$ and $d_{LS(c)}$ are the loaded side deflections under the tension and compression load, respectively.

Ideally, the difference between $\mathrm{LTE_{B(t)}}$ and $\mathrm{LTE_{B(c)}}$ shall be zero when the surface areas of the aggregates engaged in load transfer in both the directions are equal. But in reality, the developed crack is not perfectly vertical, which results in a different quantity of aggregate engagement in one direction than the other. Since the area of the crack face in a beam specimen is far lower than that of a slab specimen, a small difference in the area of the aggregate engaged in load transfer significantly influences the magnitude of the load transfer. Therefore, the average of $\mathrm{LTE_{B(t)}}$ and $\mathrm{LTE_{B(c)}}$ provides a more meaningful characterization. This average neutralizes the effect of macro texture to a certain extent.

S

The typical load and deflection profiles obtained in the $\mathrm{S_{ALT}}$ procedure are shown in Figure 3-35. It can be seen that when the approach slab load reaches the peak load, the leave slab load goes down to the minimum, and vice versa. It can be assumed that at the time when the load on a particular slab reaches the peak, the deflections on both the approach and leave slabs are due only to the load applied on that slab. It can be seen in Figure 3-35, that the time when the peak load is applied to the approach slab, peak deflection also occurs at about the same time the load peak is observed. The same occurs for the leave slab. In this procedure, a phase difference between the peak load and peak deflection can be observed, as was seen in the $\mathrm{B_{ALT}}$ due to the time-dependent response of the Fabcel.

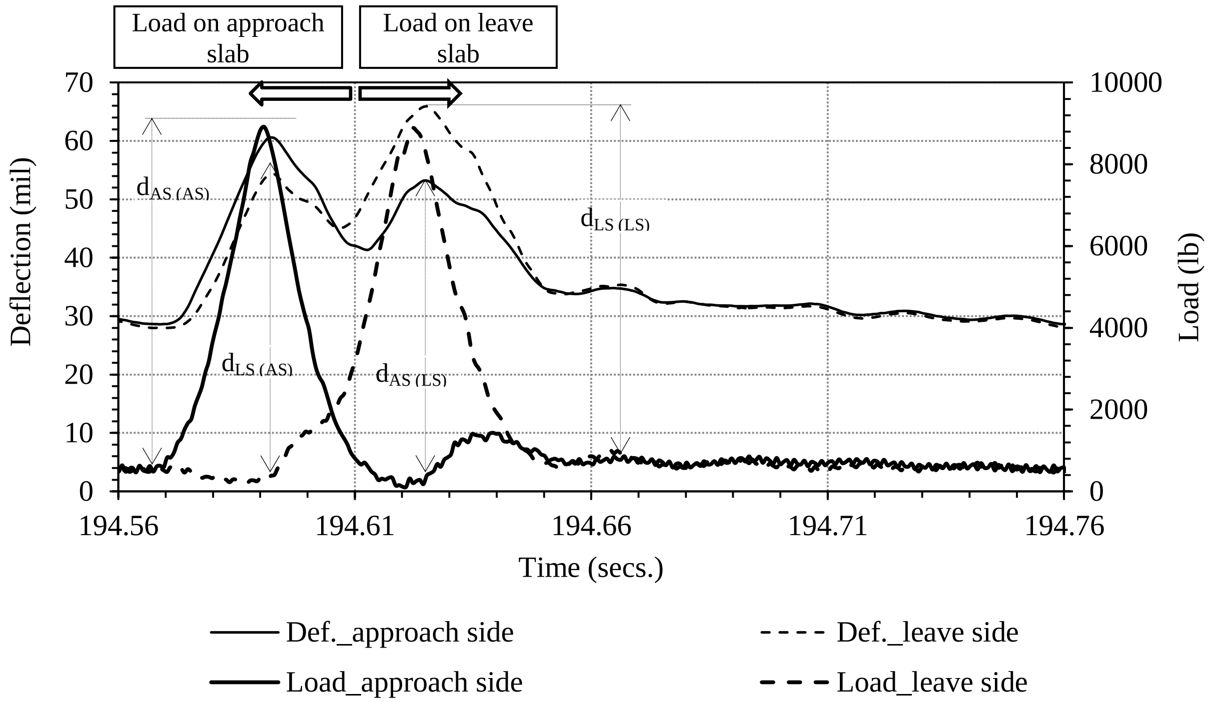

Figure 3-35: Typical load and deflection profiles for S_{ALT}.

In this case, LTE can be separately calculated for the approach and leave sides. These are calculated using the following equations.

$$\mathrm{LTE}_{\mathrm{S(A)}} = \frac{d_{L(AL)}}{d_{A(AL)}} \tag{3-6}$$

$$\mathrm{LTE}_{\mathrm{S(L)}} = \frac{d_{A(LL)}}{d_{L(LS)}} \tag{3-7}$$

where $\mathrm{LTE}_{\mathrm{S(A)}}$ and $\mathrm{LTE}_{\mathrm{S(L)}}$ are the approach and leave side LTEs; $d_{L(AL)}$ and $d_{A(AL)}$ are the deflections at the leave and approach sides, respectively, with the peak load on the approach slab; $d_{A(LL)}$ and $d_{L(LL)}$ are the deflections at the approach and leave sides, respectively, with the peak load on the leave slab.

3.4.2 Joint performance through DER

The concrete pavement system dissipates energy when it deflects under the wheel load. The magnitude of the dissipated energy (DE) is proportional to the magnitude of the pavement deflection. Conceptually, the DE is the area under the load vs deflection curve. The difference in magnitude of the DEs between the approach and leave sides is known as differential energy dissipation (DED), and the ratio between the leave side DE to the approach side DE is known as dissipated energy ratio (DER). For good joint performance, the magnitude of the DE on both sides is low with lower values of DDE and DER.

B_{ALT}

In the B_{ALT}, as was shown in Figure 3-34, the total load cycle comprises of four individual loading segments, in order, (i) 0 to -1050 lbs, (ii) -1050 to 0 lb, (iii) 0 to +1050 lbs and (iv) +1050 to 0 lb. In that figure, it is seen that at the time when the load drops from -1050 to 0 lb (at the end of the second segment), the Fabcel layers still exhibit some amount of deflection. This results in a hysteresis in the load vs deflection curve. This means the areas of the load vs deflection curves for the 0 to maximum and maximum to 0 loads are not similar; the later one has higher value. This can be seen in Figure 3-36. This figure includes load vs deflection profiles for all four segments, for deflections on both the loaded and unloaded sides. Because of the presence of the hysteresis, the areas under the load vs deflection curve for each segment are different and therefore computed separately.

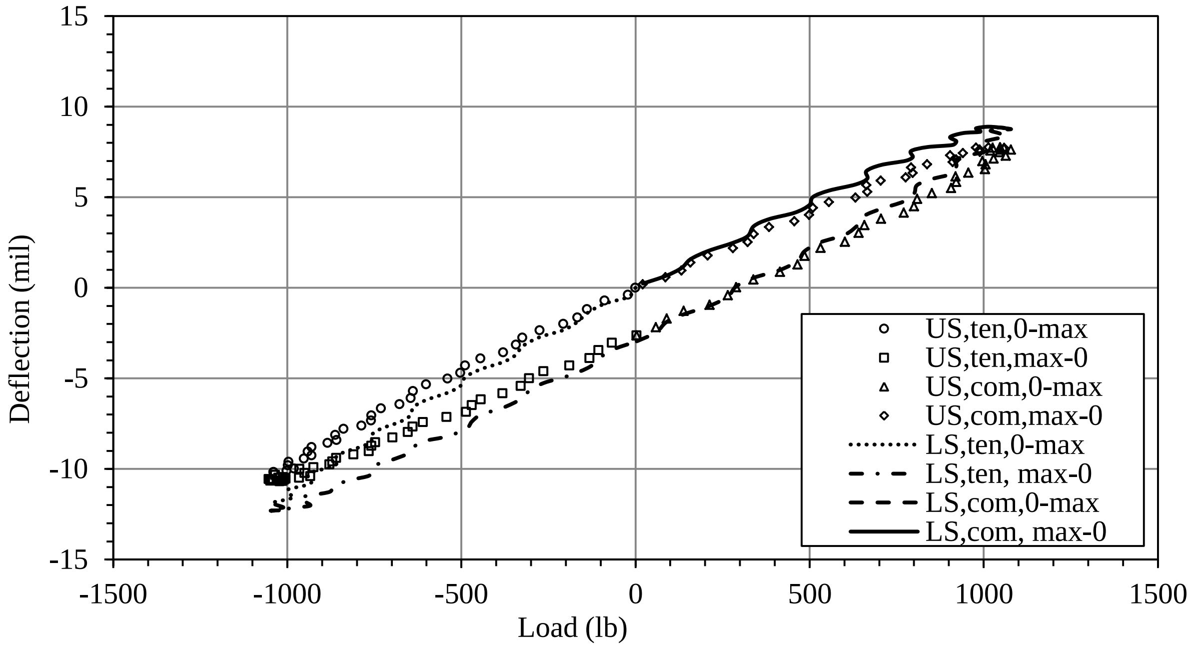

US- unloaded side; LS- loaded side; ten- tension; com- compression.

Figure 3-36: A typical load vs deflection curve for the B_{ALT}.

The total load vs deflection curve shown in Figure 3-36, is broken into eight separate segments, four each for loaded and unloaded sides, as shown in Figure 3-37. The curves for the loaded side and unloaded side are presented in plots (i) to (iv) and (v) to (viii), respectively. The area in each plot, which represents the DE, is marked as A_n (n = 1 to 8). The DE computed separately for each segment facilitates the derivation of the DED and DER separately for the tension loading and compression loading. Under the tension loading, the sum of A_1 and A_2 represents the total DE under the loaded side, whereas the sum of A_5 and A_6 represents the total DE under the unloaded side. Similarly, A_3 , A_4 , A_7 and A_8 can be used to compute the corresponding DEs for the loaded and unloaded sides, when the compression load is applied. The DED and DER in the B_{ALT} procedure can then be computed by using the following equations.

$$\mathrm{DED}_{\mathrm{B(t)}} = (A_1 + A_2) - (A_5 + A_6) \tag{3-8}$$

$$\mathrm{DED}_{\mathrm{B(c)}} = (A_3 + A_4) - (A_7 + A_8) \tag{3-9}$$

$$\mathrm{DER_{B(t)}} = \frac{(A_5 + A_6)}{(A_1 + A_2)} \tag{3-10}$$

$$\mathrm{DER_{B(c)}} = \frac{(A_7 + A_8)}{(A_3 + A_4)} \tag{3-11}$$

where $\mathrm{DED_{B(t)}}$ and $\mathrm{DED}_{B(\mathrm{c})}$ are the DED under the tension and compression loads, respectively; $\mathrm{DER_{B(t)}}$ and $\mathrm{DER_{B(c)}}$ are the DER under the tension and compression loads, respectively.

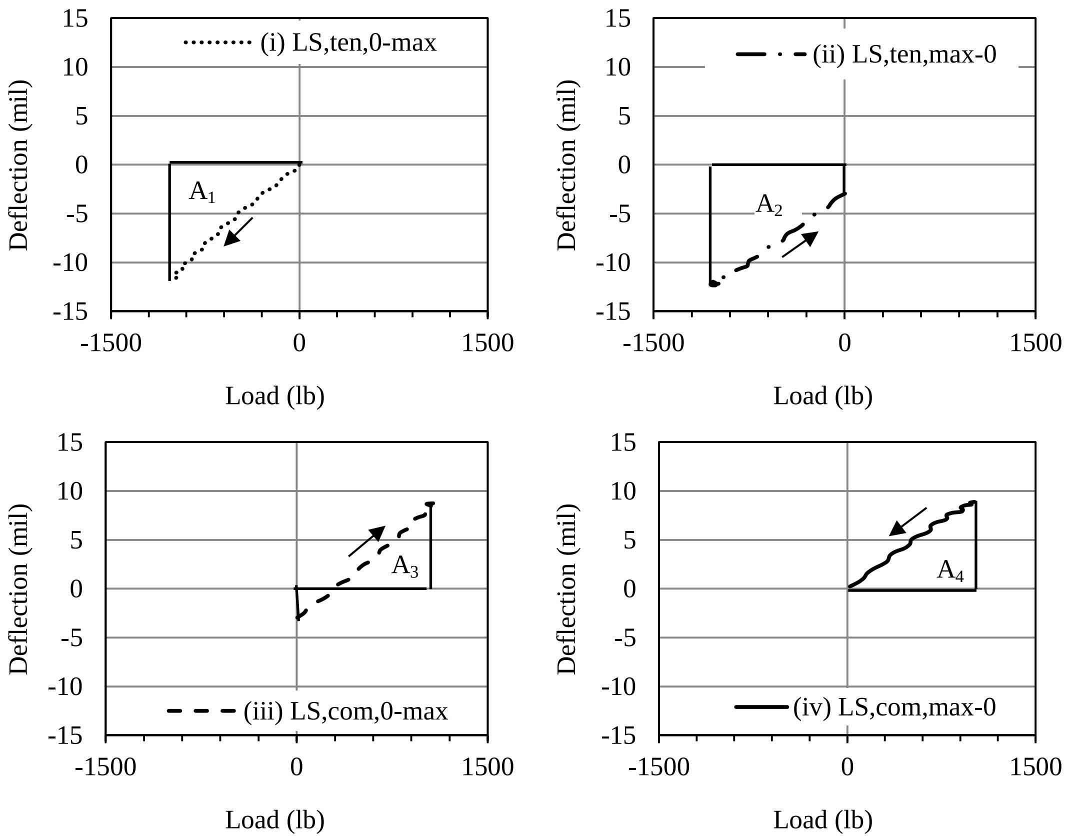

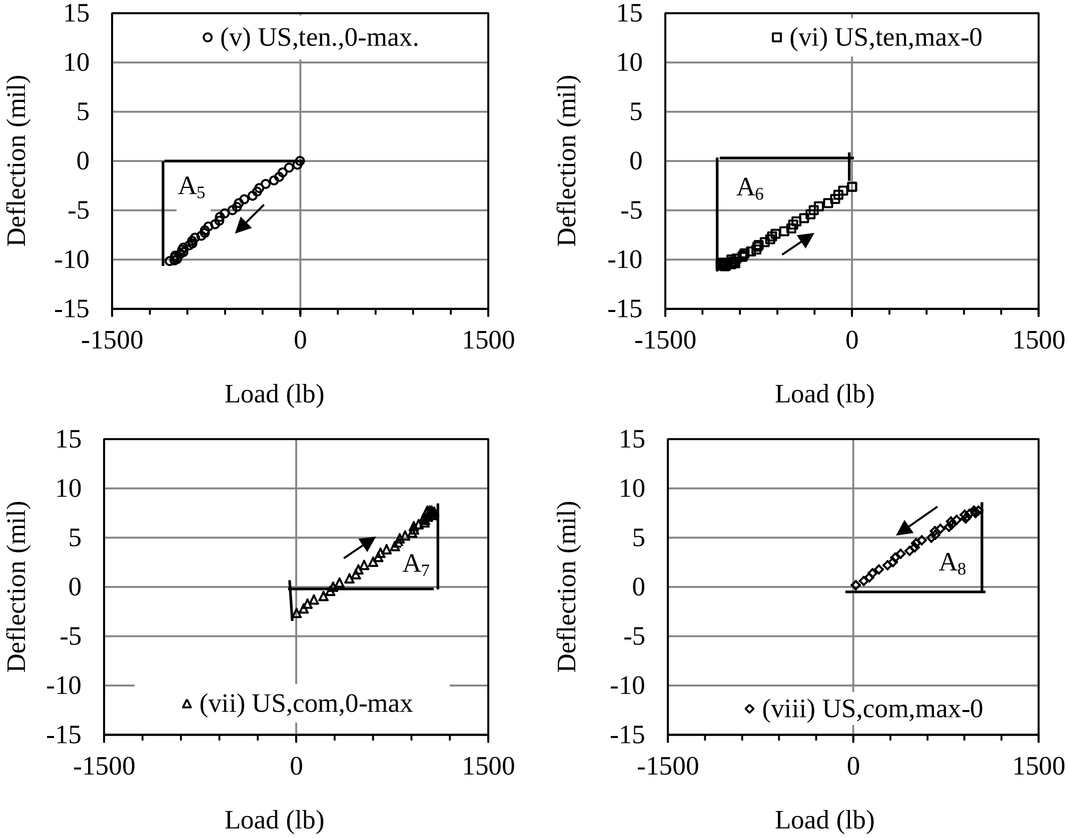

Figure 3-37: Individual segments in the load vs deflection curve: (i) to (iv) - loaded side and (v) to (viii) -unloaded side.

S_{ALT}

The load in the S_{ALT} is applied using two actuators so the derivation of DED and DER is different. In the load and deflection profiles shown in Figure 3-35, it can be seen that there is an overlap of approach and leave side loads. This occurs in the middle of the loading cycle when the load applied on the approach slab is transferred to the leave slab. In this particular case (Figure 3-35), the load on both of the actuators remains below 2000 lbs in the overlapping zone. To avoid this overlapping, deflection due to any load below 2000 lbs for either of the actuators is discarded from the analysis.

Figure 3-38 shows a deflection trace for the approach side. The deflections generated by the loads below 2000 lbs are discarded. The solid line in the graph represents the deflection when the load is applied to the approach slab, whereas the dash line shows the deflection when load is applied on the leave slab. In this graph, the deflection increases from 27 to 57 mils when the load on the approach side increases from 2000 to 9000 lbs and then drops to 44 mils when the load drops back to 2000 lbs. The difference between the deflections, at the 2000-lbs load is 17 mils. This hysteresis is due to the delay response of the Fabcel. Immediately following the deflection increases again to 54 mils as a result of the load increase on the leave slab. Figure 3-39 shows the deflection trace measured for the leave slab. Similar to the earlier graph, the solid and dash lines represent the deflection generated by the loads applied on the approach and leave slabs, respectively. As expected, the deflection on the leave side also exhibited a hysteresis. Therefore, in the S_{ALT}, DEs are also calculated separately for each different segment in the total loading cycle.

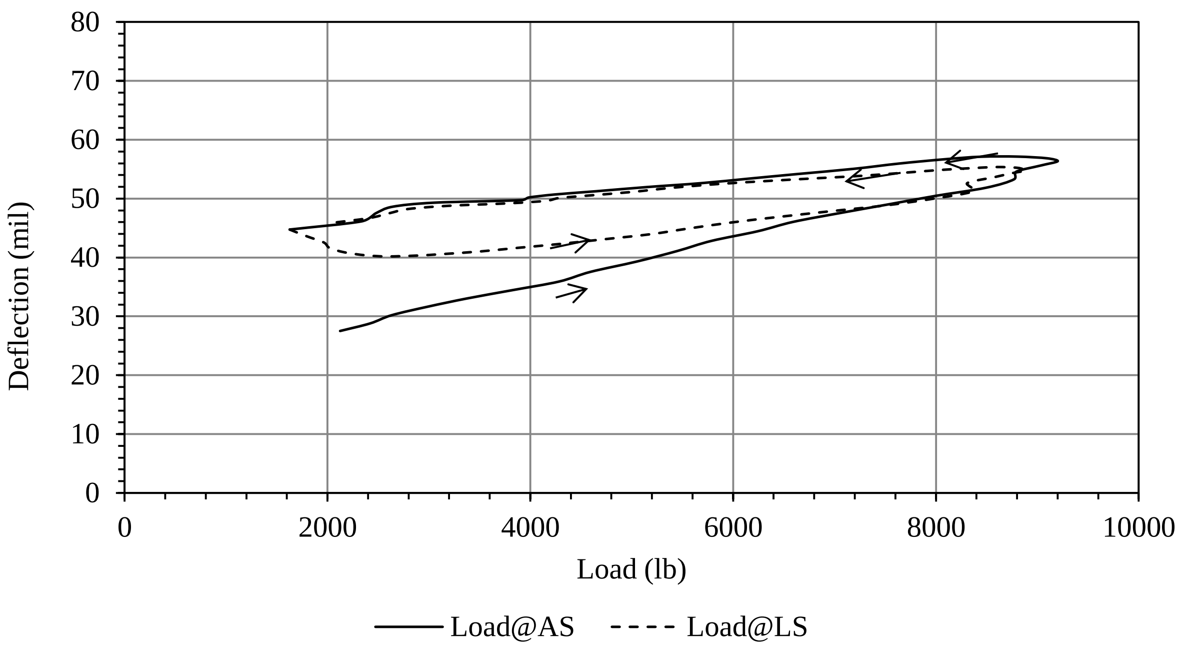

Figure 3-38: Deflection measured on the approach side.

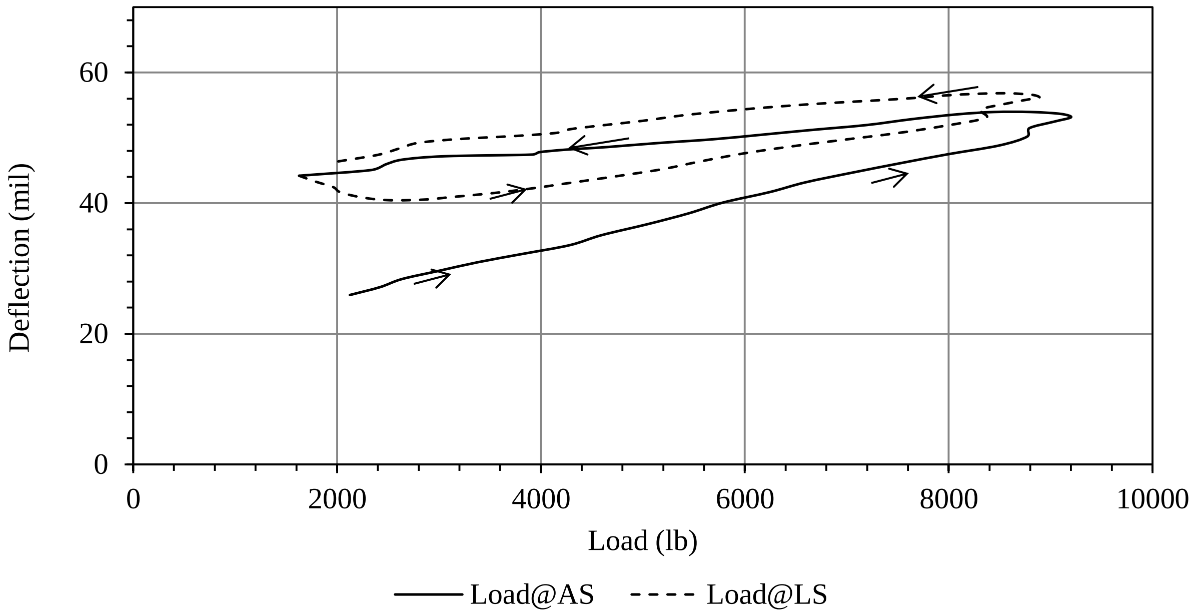

Figure 3-39: Deflection trace on the leave side.

The deflection traces shown in Figure 3-38 and Figure 3-39 are broken in to eight separate segments, four for the approach and four the leave side slabs. These are shown in Figure 3-40. The area of each segment, marked as B_n (n = 1 to 8), represents the corresponding DE for that segment. B_1 and B_2 are the DEs for the approach slab, whereas B_5 and B_6 are the DEs for the leave slab with the load being applied on the approach slab. Similarly, B_3 , B_4 , B_7 and B_8 are the DEs corresponding to the load on the leave slab. Using an approach similar to the B_{ALT} procedure, the DED and DER for the S_{ALT} are determined using the following equations.

$$\mathrm{DED}_{\mathrm{S(A)}} = (B_1 + B_2) - (B_5 + B_6) \tag{3-12}$$

$$\mathrm{DED}_{\mathrm{S(L)}} = (B_7 + B_8) - (B_3 + B_4) \tag{3-13}$$

$$\mathrm{DER}_{\mathrm{S(A)}} = \frac{(B_5 + B_6)}{(B_1 + B_2)} \tag{3-14}$$

$$\mathrm{DER}_{\mathrm{S(L)}} = \frac{(B_3 + B_4)}{(B_7 + B_8)} \tag{3-15}$$

where $DED_{S(A)}$ and $DED_{S(L)}$ are the DED for the approach and leave slabs, respectively; $DER_{S(A)}$ and $DER_{S(L)}$ are the DER for the approach and leave slabs, respectively.

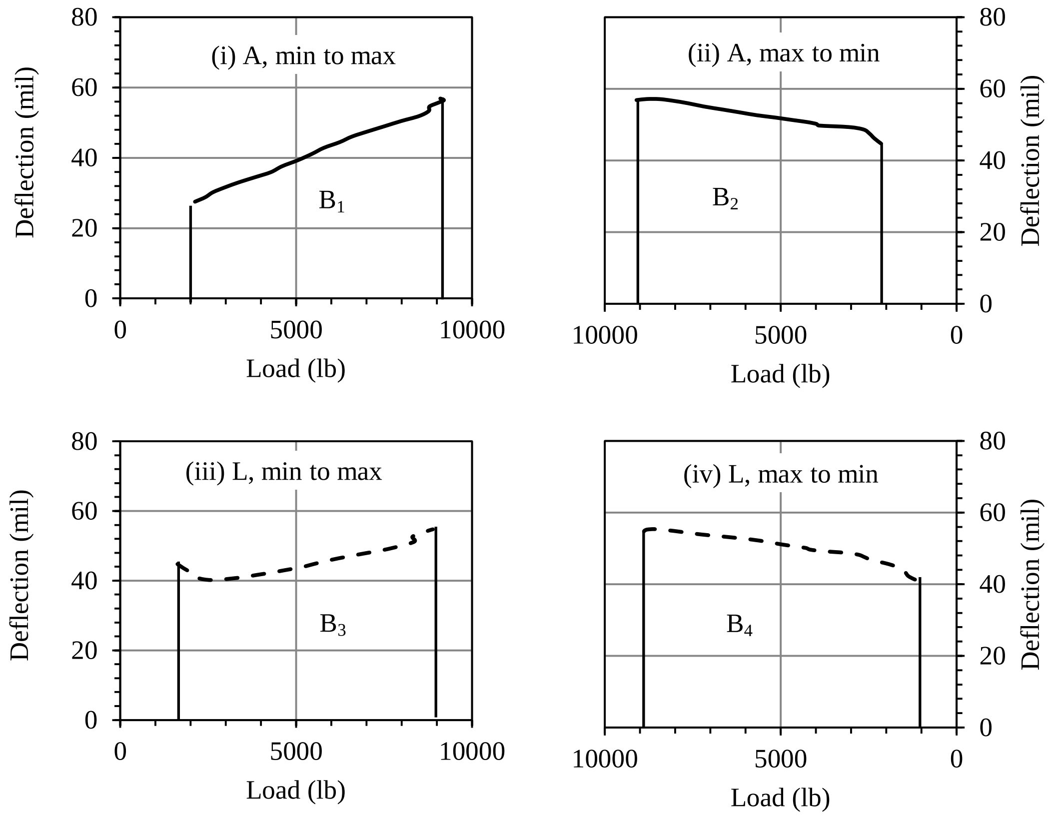

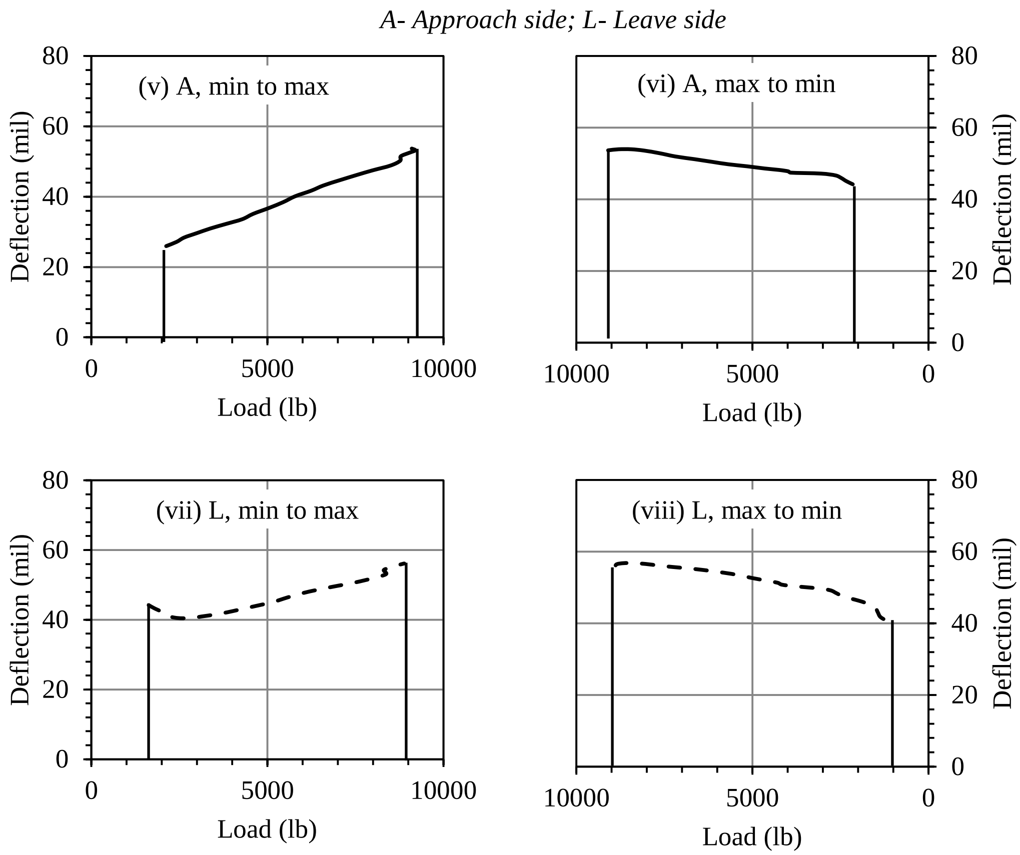

Figure 3-40: Individual segments in the S_{ALT} load vs deflection curve: (i) to (iv) - load on the approach side and (v) to (viii) - load on the leave side.

3.5 Conclusions

This chapter presented a comprehensive detail of the two joint performance test setups built under the scope of the present study. Although both the methods were developed to evaluate the joint performance for a whitetopping overlay, the joint performance for any concrete pavement is also possible using either method. Evaluation of the joint performance with the B_{ALT} procedure is very economic and faster. This setup can be very helpful to characterize joint performance when a large numbers of variables are to be considered. The S_{ALT} is more expensive but simulates the pavement joint condition in a more realistic manner.